# mTORC2 promotes cell survival through c-Myc–dependent up-regulation of E2F1

Zhipeng Zou,[1]* Juan Chen,[1]* Anling Liu,[1] Xuan Zhou,[1] Qiancheng Song,[1] Chunhong Jia,[1] Zhenguo Chen,[1] Jun Lin,[1] Cuilan Yang,[1] Ming Li,[1] Yu Jiang,[2] and Xiaochun Bai[1]

[1]Department of Cell Biology, School of Basic Medical Sciences, Southern Medical University, Guangzhou, Guangdong 510515, China
[2]Department of Pharmacology and Chemical Biology, University of Pittsburgh School of Medicine, Pittsburgh, PA 15213

Previous studies have reported that mTORC2 promotes cell survival through phosphorylating AKT and enhancing its activity. We reveal another mechanism by which mTORC2 controls apoptosis. Inactivation of mTORC2 promotes binding of CIP2A to PP2A, leading to reduced PP2A activity toward c-Myc serine 62 and, consequently, enhancement of c-Myc phosphorylation and expression. Increased c-Myc activity induces transcription of *pri-miR-9-2/miR-9-3p*, in turn inhibiting expression of E2F1, a transcriptional factor critical for cancer cell survival and tumor progression, resulting in enhanced apoptosis. In vivo experiments using B cell–specific mTORC2 (rapamycin-insensitive companion of mTOR) deletion mice and a xenograft tumor model confirmed that inactivation of mTORC2 causes up-regulation of c-Myc and *miR-9-3p*, down-regulation of E2F1, and consequent reduction in cell survival. Conversely, *Antagomir-9-3p* reversed mTORC1/2 inhibitor–potentiated E2F1 suppression and resultant apoptosis in xenograft tumors. Our in vitro and in vivo findings collectively demonstrate that mTORC2 promotes cell survival by stimulating E2F1 expression through a c-Myc– and *miR-9-3p*–dependent mechanism.

## Introduction

The evolutionarily conserved mechanistic target of rapamycin (mTOR) forms two functionally distinct complexes. The first, mTORC1, consisting of mTOR, regulatory-associated protein of mTOR (Raptor), and mLST8 (GβL), is sensitive to rapamycin and thought to control autonomous cell growth in response to nutrient availability and growth factors. The second complex, mTORC2, containing the core components mTOR, mSIN1, mLST8, and rapamycin-insensitive companion of mTOR (Rictor), is largely insensitive to rapamycin (Ma and Blenis, 2009; Laplante and Sabatini, 2012; Jewell et al., 2013; Johnson et al., 2013). mTORC2 was discovered more recently, and limited information is available on its regulation and function. Phosphorylation of Akt at the hydrophobic motif site (Ser 473) necessary for activity toward some (but not all) substrates is the best characterized readout of mTORC2 activity (Sarbassov et al., 2005; Laplante and Sabatini, 2012). Studies to date suggest that mTORC2 specifically senses growth factors and regulates proliferation, actin cytoskeleton, and cell survival. However, inconsistent findings have been reported, and the underlying mechanisms are currently unclear (Oh and Jacinto, 2011; Hung et al., 2012).

Dysregulation of mTOR signaling often occurs in a variety of human malignant diseases, making it a crucial validated target in cancer treatment (Bai and Jiang, 2010; Dancey, 2010). However, the effectiveness of rapamycin as a single-agent therapy is suppressed, in part, by the numerous strong mTORC1-dependent negative feedback loops. mTORC1 inhibition stimulates Akt via activation of the IRS-1–PI3-K–PDK1 pathway to promote cell survival (Benjamin et al., 2011; Carew et al., 2011; Wander et al., 2011). Although preclinical studies with ATP-competitive mTOR inhibitors that target both mTORC1 and mTORC2 have disclosed greater effectiveness of these compounds than rapalogs in cancer treatment, questions regarding their efficacy remain (Feldman et al., 2009; Wander et al., 2011). mTORC2 inhibition does not affect the feedback activation of PI3-K–PDK1 and Akt (Threonine 308) induced by mTORC1 inhibition, which may be sufficient to drive cell survival. Another major concern is whether these catalytic inhibitors will be tolerated (Benjamin et al., 2011; Carew et al., 2011; Wander et al., 2011). Recent cancer biology studies indicate mTORC2 as a promising target because its activity is essential for the development of a number of cancers (Sparks and Guertin, 2010; Benjamin et al., 2011). Data from these studies provide a rationale for developing inhibitors specifically targeting mTORC2, which do not perturb the mTORC1-dependent

*Z. Zou and J. Chen contributed equally to this paper.

Correspondence to Xiaochun Bai: baixc15@smu.edu.cn

Abbreviations used in this paper: 5-FU, 5-fluorouracil; CA, constitutively active; ChIP, chromatin immunoprecipitation; DN, dominant-negative; KO, knockout; mTOR, mechanistic target of rapamycin; OA, okadaic acid; PARP, poly (ADP-ribose) polymerase; Raptor, regulatory-associated protein of mTOR; Rictor, rapamycin-insensitive companion of mTOR; UTR, untranslated region; WT, wild type; RT-qPCR, quantitative RT-PCR.



The Rockefeller University Press $30.00
J. Cell Biol. Vol. 211 No. 1 105–122
www.jcb.org/cgi/doi/10.1083/jcb.201411128

negative feedback loops and have a more acceptable therapeutic window (Sparks and Guertin, 2010; Benjamin et al., 2011). However, the 3D structure of mTORC2, its precise role in cell survival regulation, and underlying mechanisms of action remain to be clarified (Sparks and Guertin, 2010; Oh and Jacinto, 2011; Hung et al., 2012).

Resistance to apoptosis is essential for cancer growth and appears to be the major cause of therapeutic failure. The transcription factor, E2F1, plays a critical role in cell cycle progression and induction of apoptosis in response to DNA damage (Stanelle and Pützer, 2006; Biswas and Johnson, 2012). Recent evidence has shown that this tumor suppressor is aberrantly expressed in late-stage cancers and is relevant for cancer progression and genotoxic drug resistance (Engelmann and Pützer, 2012; Pützer and Engelmann, 2013). Increased abundance of E2F1 triggers invasion and metastasis via activation of growth receptor signaling pathways, which, in turn, promote an anti-apoptotic tumor environment (Ladu et al., 2008; Zheng et al., 2009; Engelmann and Pützer, 2012). Thus, identification and functional characterization of the signaling networks that govern E2F1 expression and activity is necessary to develop new therapeutic strategies for overcoming chemoresistance.

Recently, miRNAs have emerged as modulators of biological pathways essential for cancer initiation, development, and progression. Two studies suggest that miRNAs act as either tumor suppressors or oncogenes (Ma et al., 2010; Pencheva and Tavazoie, 2013). miRNAs may also be used as biomarkers of response to chemotherapy, given their important roles in cancer cell survival and drug resistance (Thum et al., 2008; Ma et al., 2010; Pencheva and Tavazoie, 2013). Antagomirs that suppress miRNA expression are currently being tested in cancer therapy (Wahlquist et al., 2014). mTOR and its signaling pathways are reported to be regulated by miRNAs (Uesugi et al., 2011; AlQurashi et al., 2013; Jin et al., 2013). Additionally, mTORC1 regulates miRNAs that play critical roles in cell proliferation, differentiation, and survival (Sun et al., 2010; Totary-Jain and Marks, 2013; Trindade et al., 2013). However, the miRNAs specifically regulated by mTORC2 and their roles in cell survival have yet to be established. In the present study, we show that mTORC2 negatively regulates *miR-9-3p* (also known as *miR-9**) to enhance E2F1 expression and promote cell survival via a c-Myc–dependent mechanism. Conversely, mTORC2 inhibition or deletion stimulates the expression of *miR-9-3p*, which directly targets E2F1, leading to enhanced genotoxic drug–induced apoptosis.

## Results

### *miR-9-3p* is a proapoptotic miRNA specifically up-regulated by PP242, but not rapamycin

To identify the miRNAs regulated by mTORC1 and mTORC2, a global miRNA expression profile (959 miRNAs in total) in MCF-7 cells treated with rapamycin (mTORC1 inhibitor) or PP242 (mTORC1/2 kinase inhibitor) was developed using microarray. Expression patterns of miRNAs in PP242-treated cells were considerably different from those of rapamycin-treated cells, indicating differential regulation by mTORC1 and mTORC2 (Fig. 1 A). After excluding miRNAs that were expressed at extremely low levels or statistically not significant (less than threefold), we identified 22 and 20 differentially expressed miRNAs in rapamycin- and PP242-treated cells, respectively, compared with control cells (Fig. 1 B). The levels of eight miRNAs in PP242-treated cells differed significantly from both rapamycin-treated and control cells, indicating specific modulation by mTORC2 (Table S1). We subsequently examined the roles of these miRNAs in cell survival by transfecting MCF-7 cells with the respective mimics. Interestingly, only *miR-9-3p* significantly promoted serum deprivation and cisplatin-induced cell death (Fig. 1 C), implying a potential role in mediating mTORC2 inhibition–related apoptosis. Quantitative RT-PCR (RT-qPCR) experiments further confirmed up-regulation of *miR-9-3p* by PP242, but not by rapamycin, in MCF-7, A549, and MDA-MB-231 cells (Fig. 1 D).

*miR-9-5p* and *miR-9-3p* are mature products from each strand of the same pri-miR-9 hairpin RNA structure that have different sequences and target mRNAs with distinct functions. *miR-9-5p* has been widely investigated as an oncogenic miRNA and shown to play critical roles in the pathogenesis and metastasis of human cancers (Ma et al., 2010; Yuva-Aydemir et al., 2011; Chen et al., 2013). However, the function of *miR-9-3p* is not clear at present (Jeon et al., 2011; Heller et al., 2012; Zawistowski et al., 2013). To determine the specific roles of *miR-9-3p* and *miR-9-5p* in apoptosis, miRNA mimics were introduced into MCF-7 cells. As evident from cell morphology, viability, cleavage of poly (ADP-ribose) polymerase (PARP; cleavage by active caspase-3 is widely accepted as a hallmark of late-stage apoptosis but not necrosis; Fig. 1 E), and the Annexin V–FITC apoptosis assay (Fig. S1 A), *miR-9-3p*, but not *miR-9-5p* (Fig. S2, A and B), induced an increase in apoptosis, both in the absence and presence of serum starvation and low-dose 5-fluorouracil (5-FU), a widely used genotoxic drug, in a dose-dependent manner. The proapoptotic function of *miR-9-3p* was further confirmed in MDA-MB-231 (Fig. 1 F and Fig. S1 A) and other cell lines (Fig. S1 B). Furthermore, antagomir of *miR-9-3p*, but not that of *miR-9-5p* (Fig. S2, C and D), suppressed serum starvation and 5-FU–induced apoptosis in MCF-7 (Fig. 1 G) and MDA-MB-231 cells (Fig. 1 H). These results collectively support the finding that *miR-9-3p* is a proapoptotic miRNA regulated by mTORC2.

### mTORC2, but not mTORC1, negatively regulates *miR-9-3p* to promote cell survival

To directly confirm whether mTORC2 influences the *miR-9-3p* level, we eliminated Rictor or Raptor using siRNAs with two independent target sequences inhibiting Akt (Ser 473) and S6 (Ser 235/236) phosphorylation (the key hallmarks of mTORC1 and mTORC2 activation, respectively; Fig. 2 A, right). Mature *miR-9-3p* expression was induced upon Rictor, but not Raptor knockdown, as shown using RT-qPCR (Fig. 2 A, left). In addition, Northern blot analysis confirmed that both precursor and mature *miR-9-3p* are induced upon mTORC2 but not mTORC1 inhibition (Fig. 2 B). Furthermore, under serum deprivation, which represses mTORC1/2 activity, the *miR-9-3p* level was enhanced (Fig. 2 C, left), whereas amino acid starvation that specifically blocks mTORC1 had little effect on *miR-9-3p* (Fig. 2 C, right). These results clearly demonstrate that *miR-9-3p* is negatively regulated by mTORC2, but not mTORC1.

To ascertain the potential role of *miR-9-3p* in mTORC2-regulated cell survival, we examined the effect of the *miR-9-3p*–specific antagomir on PP242-stimulated cell death. As expected, the antagomir induced a decrease in the

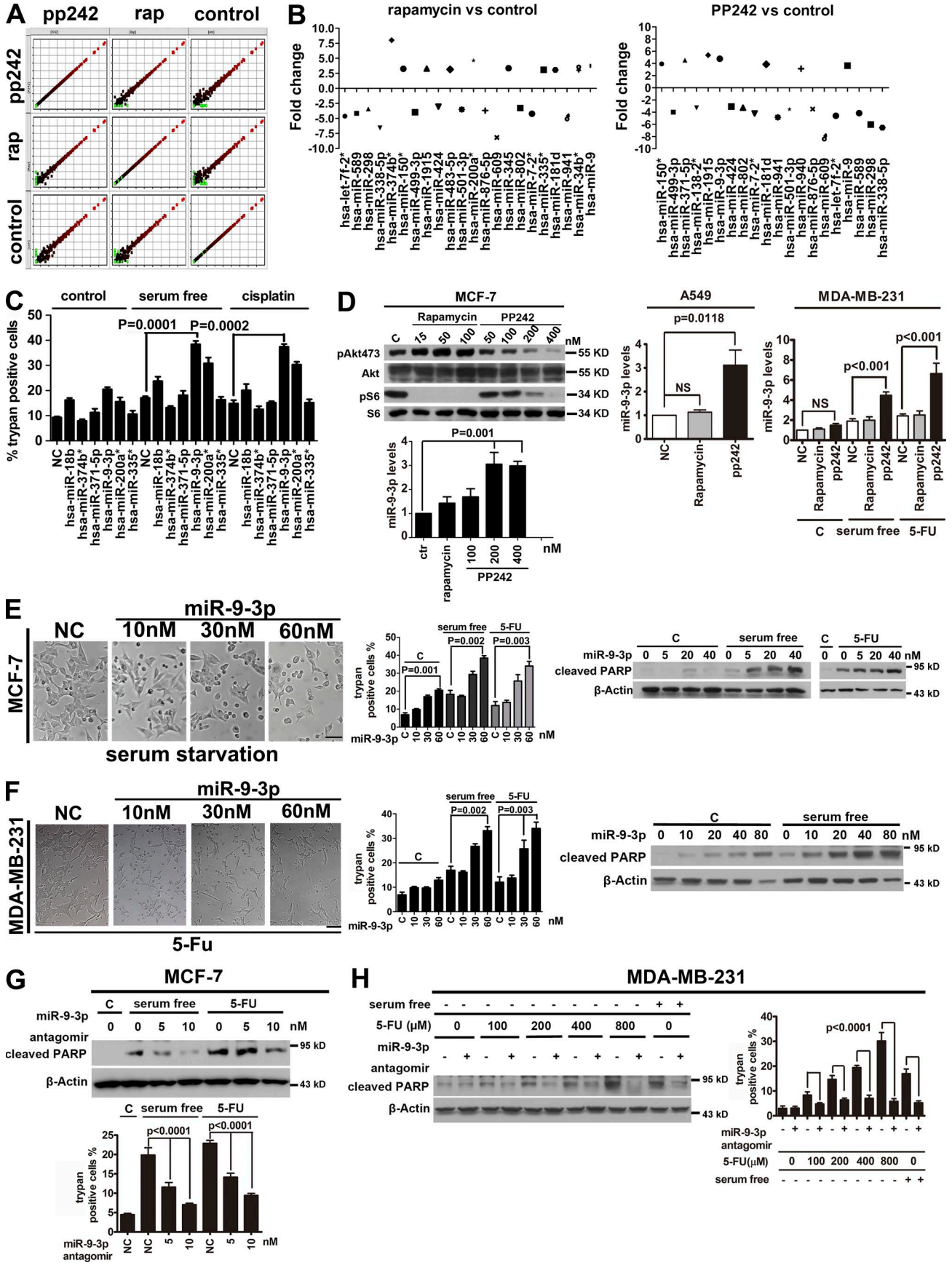

PP242-enhanced apoptotic cell number (Fig. 2 D) and cleavage of PARP (Fig. 2 E). These lines of evidence suggest that *miR-9-3p* is a negative regulatory target of mTORC2 that functions to promote cell survival.

### E2F1, a novel target of *miR-9-3p*, is up-regulated by mTORC2 to promote cell survival

The capacity of *miR-9-3p* to promote apoptosis may be derived from its ability to target genes involved in cell survival. We applied two algorithms that predict the mRNA targets of miRNAs, specifically PicTar and TargetScan (Krek et al., 2005). Based on the seed region in their 3′ untranslated regions (UTRs), >100 mRNAs were predicted to be regulated by *miR-9-3p* (unpublished data). Among them, E2F1, E2F3, MDM2, and PDK1 are involved in regulating apoptosis (Westmoreland et al., 2009; Martinez et al., 2010; Kurokawa et al., 2013; Pützer and Engelmann, 2013) and closely related to mTOR. To screen the potential targets of *miR-9-3p*, we cloned the 3′ UTR of E2F1, E2F3, MDM2, and PDK1 into a luciferase construct (Fig. 3 A). Reporter assays using *miR-9-3p*–expressing MCF-7 cells showed that *miR-9-3p* suppresses the expression of E2F1 (Fig. 3 B, top), but not that of E2F3, MDM2, or PDK1 (Fig. 3 B, bottom). Furthermore, mutation of the putative *miR-9-3p* seed region in the 3′ UTR of E2F1 abrogated responsiveness to *miR-9-3p* (Fig. 3 B, top). Consistent with this finding, we observed a clear decrease in endogenous E2F1 mRNA and protein levels in MCF-7 cells transfected with *miR-9-3p* mimics. Conversely, the antagomir of *miR-9-3p* induced a significant increase in the E2F1 mRNA and protein expression levels (Fig. 3 C). Notably, PP242, but not rapamycin, suppressed E2F1 mRNA (Fig. 3 D, left) and protein levels (Fig. 3 D, top right), similar to *miR-9-3p*, while the *miR-9-3p* antagomir restored E2F1 protein expression suppressed by PP242 (Fig. 3 D, bottom right).

We further validated the role of E2F1 in mediating mTORC2 and *miR-9-3p*–modulated cell survival. Knockdown of E2F1 with siRNAs increased serum starvation and 5-FU–stimulated apoptosis in MCF-7 cells (Fig. 4, A and B; and Fig. S3 A), whereas E2F1 overexpression suppressed PP242- or Rictor knockdown–induced apoptosis (Fig. 4, C and D; and Fig. S3 B). E2F1 overexpression rendered cells resistant to *miR-9-3p*–potentiated apoptosis (Fig. 4 E and Fig. S3 B). Additionally, ectopic E2F1 suppressed *miR-9-3p*– or Rictor knockdown–induced apoptosis in MDA-MB-231 cells (Fig. S3 C). Collectively, our results indicate that E2F1 is a novel target of the proapoptotic *miR-9-3p*. Moreover, mTORC2 promotes cell survival via inhibition of *miR-9-3p* and up-regulation of E2F1.

### Inhibition of mTORC2 modulates *pri-miR-9-2/miR-9-3p*/E2F1 expression and apoptosis in a c-Myc–dependent and Akt-independent manner

Next, we explored the mechanism underlying mTORC2-mediated regulation of *miR-9-3p* expression. Previous studies have reported that *miR-9-5p* is modulated by c-Myc (Ma et al., 2010), a key transcription factor that stimulates cell proliferation in the presence of the appropriate survival factors and promotes apoptosis in their absence (Rohn et al., 1998). Furthermore, c-Myc has been shown to interact with the promoter region of *hsa-miR-9-3*, one of the three *miR-9-3p/5p* encoding genes, thereby activating transcription of *miR-9-5p* (Ma et al., 2010). No direct evidence exists on whether c-Myc activates the transcription of *miR-9-3p*. Surprisingly, the predominant primary transcript of *miR-9-3p/5p* is *pri-miR-9-2* from *hsa-miR-9-2*, whereas *pri-miR-9-1* and *pri-miR-9-3* levels are below the detection limit (unpublished data). In addition, knockdown of c-Myc did not induce any significant decreases in both *pri-miR-9-2* and mature *miR-9-3p* in MCF-7 cells (Fig. 5 A), suggesting that the physiological c-Myc level does not contribute significantly to *miR-9-3p* transcription. Interestingly, inhibition of mTORC2 via PP242 or Rictor knockdown enhanced the c-Myc protein level, whereas inactivation of mTORC1 via rapamycin or Raptor knockdown had little effect on c-Myc expression (Fig. 5 B). Consistently, PP242, but not rapamycin, dramatically enhanced the interactions of c-Myc with two potential binding sites (A and B) located at the promoter region of *hsa-miR-9-2* (Fig. 5 C) but had minimal effects on interactions with the other two *miR-9-3p/5p*–encoding genes, *hsa-miR-9-1* and *hsa-miR-9-3* (unpublished data). These findings demonstrate that mTORC2 controls c-Myc expression and support the involvement of c-Myc in mTORC2-mediated regulation of *miR-9-3p* and cell survival.

We further examined whether mTORC2 modulates *pri-miR-9-2*/*miR-9-3p*/E2F1 through c-Myc activity. Notably, c-Myc knockdown significantly suppressed *pri-miR-9-2* and *miR-9-3p* induction by PP242 or Rictor depletion (Fig. 5, D and E). Knockdown of c-Myc additionally prevented mTORC2 inhibition–potentiated apoptosis in MCF-7 (Fig. 5, F–I) and MDA-MB-231 cells (Fig. 5 J), suggesting that mTORC2 regulates *pri-miR-9-2*/*miR-9-3p*/E2F1 expression and cell survival via down-regulation of c-Myc.

Akt is the only established mTORC2 substrate that functions in cell survival control. However, mTORC2 has been shown to mediate limited prosurvival effects of Akt (Oh and Jacinto, 2011; Hung et al., 2012; Laplante and Sabatini, 2012). The extent to which mTORC2 potentiates cell survival via Akt remains unclear. To clarify this issue, we examined whether Akt is involved in regulation of c-Myc/*miR-9-3p* by mTORC2. Transfection of MCF-7 cells with a dominant-negative (DN)

Figure 1. **miRNAs are differentially regulated by mTORC1 and mTORC2, and *miR-9-3p* is a proapoptotic miRNA induced by pp242 in multiple cell lines.** (A) MCF-7 cells were treated with control, 200-nM PP242, or 100-nM rapamycin, and after 48 h total miRNAs were analyzed with microarray. This experiment was completed once. Differential expression patterns of miRNAs between the groups are shown using a matrix plot. (B) PP242 and rapamycin-responsive miRNAs (at least threefold changes in expression vs. control) are presented. (C) Mimics of several miRNAs were transfected into MCF-7 cells, followed by 20-µM cisplatin treatment or serum starvation for 24 h, and consequent cell death was monitored using trypan blue staining. (D) *miR-9-3p* levels of MCF-7, A549, and MDA-MB-231 cells subjected to PP242 or rapamycin treatment were assayed using RT-qPCR to verify microarray results. Phosphorylated S6 and Akt were additionally monitored using Western blotting to ensure effective and specific treatment. (E and F) MCF-7 (E) and MDA-MB-231 (F) cells were transfected with *miR-9-3p* mimics at different concentrations as indicated and subsequently left untreated or subjected to serum starvation or 5-FU exposure. 60 h after transfection, cells were imaged using a light microscope (left), detached with trypsin, and monitored using trypan blue staining (middle) or harvested and analyzed via Western blotting for PARP cleavage (right). Bars, 50 µm. (G and H) MCF-7 (G) and MDA-MB-231 (H) cells were transfected with *miR-9-3p* antagomir at various concentrations and either analyzed for PARP cleavage or death rate, as indicated. Error bars represent mean values ± SEM. C, control; ctr, control; NC, negative control.

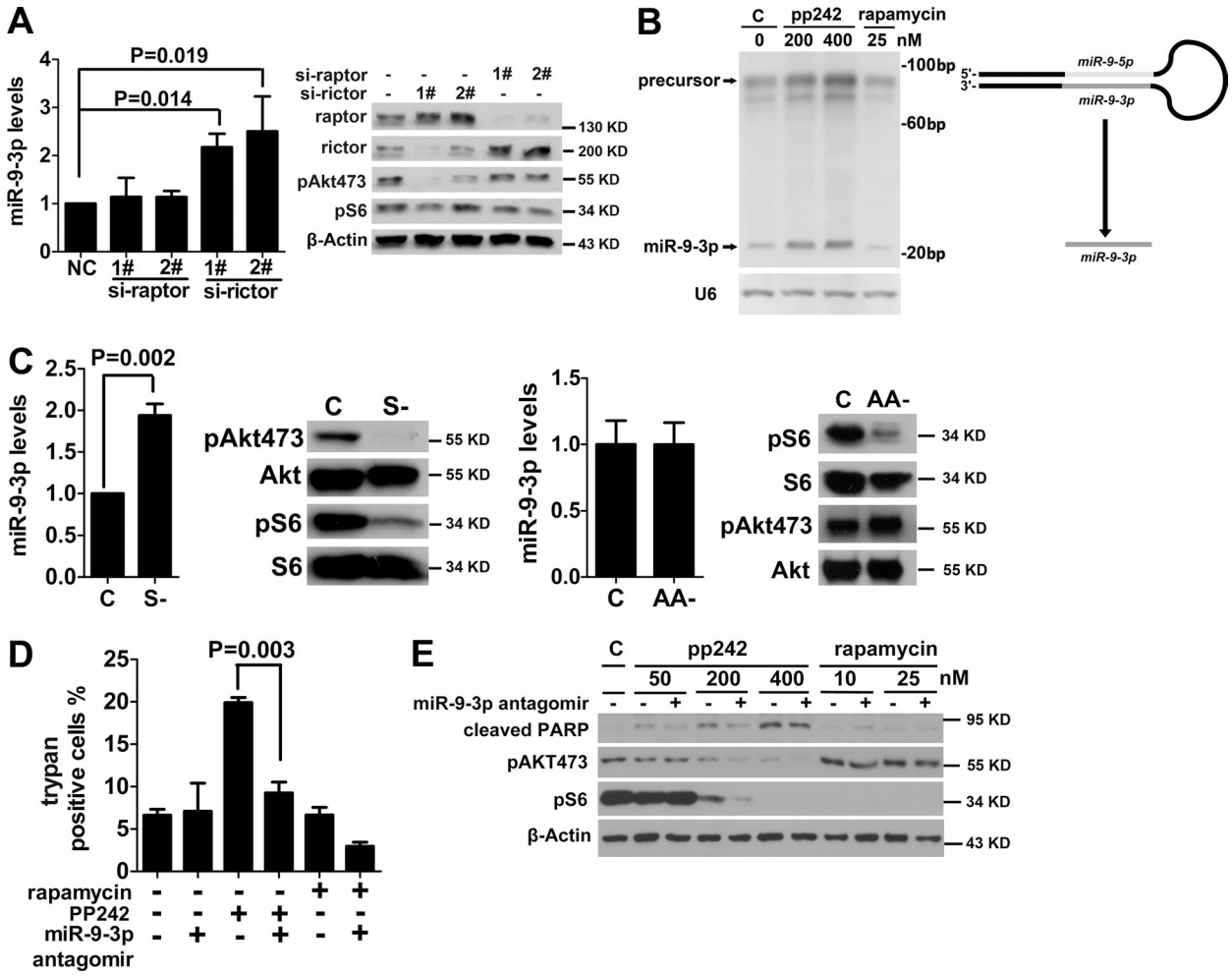


Figure 2. **mTORC2, but not mTORC1, suppresses *miR-9-3p* to promote cell survival.** (A) MCF-7 cells were transfected with nontargeted siRNA (NC) or two siRNAs targeting different regions of Rictor or Raptor mRNA. After 60 h, cells were harvested and lysed, and the *miR-9-3p* level was monitored using RT-qPCR (left). Expression of Rictor or Raptor and phosphorylation of S6 or Akt were assessed using Western blotting to ensure siRNA-induced depletion and inhibition of mTORC1 or mTORC2 (right). (B) MCF-7 cells were treated with either pp242 or rapamycin as indicated. At 24 h after treatment, *miR-9-3p* and its precursor were detected by Northern blotting. (C) MCF-7 cells were subjected to serum (left) or amino acid (AA; right) starvation, and the *miR-9-3p* level was analyzed along with S6 or Akt phosphorylation. MCF-7 cells transfected with the *miR-9-3p* antagomir were treated with PP242 or rapamycin, as indicated. (D and E) 48 h after transfection, cells were assayed for apoptosis via trypan blue staining (D) or PARP cleavage using Western blotting (E). Error bars represent mean values ± SEM. C, control; NC, negative control; S, serum.

mutant of Akt increased c-Myc and *miR-9-3p* expression only moderately and did not induce apoptosis significantly, as estimated based on unchanged levels of cleaved PARP (Fig. 6, A and B). Most importantly, although transfection with a constitutively active (CA) form of Akt managed to reactivate Akt to the full extent, as determined from the high level of phosphorylation of Akt (Ser 473), it failed to suppress the significant increase in c-Myc/*miR-9-3p* and PARP cleavage triggered by PP242 treatment (Fig. 6, A and B), indicating that the c-Myc/*miR-9-3p* proapoptotic pathway stimulated upon mTORC2 inhibition is not attributed to accompanying Akt inhibition. Further analysis of the cotransfected cell fraction sorted via FACS (Kovala et al., 2000) confirmed that ectopic expression of Akt-CA did not reverse escalation of the c-Myc/*pri-miR-9-2*/*miR-9-3p* levels and PARP cleavage stimulated by PP242 (Fig. 6, C and D). Conversely, knockdown of endogenous Akt1 led to a moderate increase in PARP cleavage in MCF-7 and A549 cells, suggesting a potential prosurvival role in these cells, but had little effect on c-Myc/*pri-miR-9-2*/*miR-9-3p* levels (Fig. 6, E–H). These findings collectively indicate that the mTORC2/c-Myc/*pri-miR-9-2*/*miR-9-3p* proapoptotic cascade is Akt independent.

### mTORC2 suppresses c-Myc/*miR-9-3p* through CIP2A/PP2A-mediated dephosphorylation at serine 62 (S62) of c-Myc

In our experiments, a slight molecular upshift of c-Myc was observed upon depletion of Rictor or inhibition of mTORC2 (Fig. 5, H and I), indicating that mTORC2 mediates dephosphorylation of c-Myc at some sites. Because phosphorylation of c-Myc at S62 appears pivotal for c-Myc stability and transcriptional activity (Yeh et al., 2004), we examined whether mTORC2 affects phosphorylation at this site. Remarkably, silencing of Rictor or treating cells with PP242 significantly enhanced c-Myc S62 phosphorylation relative to total c-Myc levels in MCF-7, MDA-MB-231, and HCT-116 cells (p53 mutant subtype; Fig. 7 A and Fig. S4, A–C). Considering the finding that PP2A interacts with c-Myc and is involved in S62

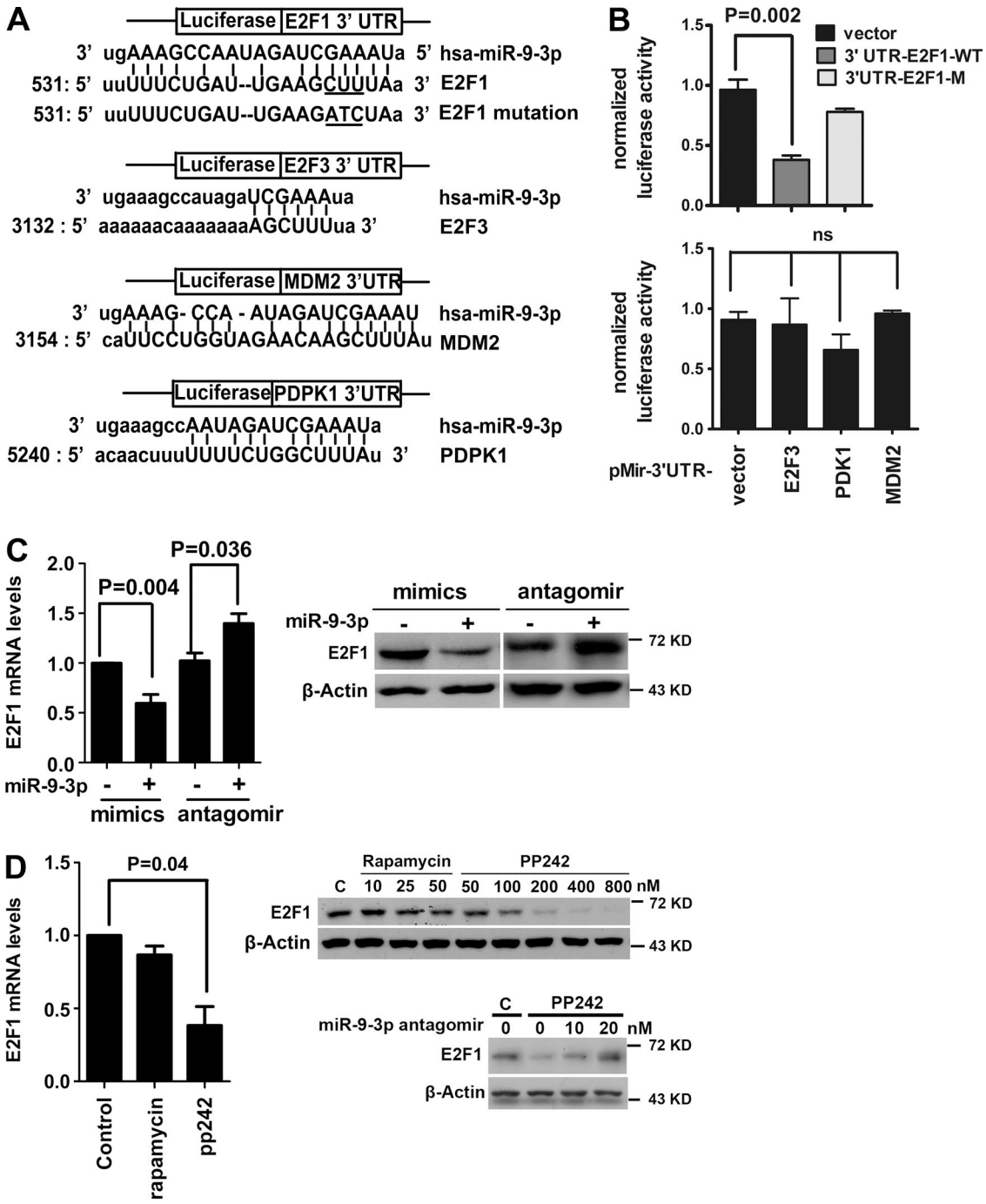


Figure 3. ***miR-9-3p* down-regulates E2F1 by directly targeting its 3′ UTR.** (A) WT 3′ UTR of E2F1, E2F3, MDM2, or PDK1 or mutant 3′ UTR of E2F1 mRNA was cloned into pMIR-REPORT downstream of Firefly luciferase, and the resulting plasmid was designated pMIR-3′-UTR-E2F1, pMIR-3′-UTR-E2F3, pMIR-3′-UTR-MDM2, pMIR-3′-UTR-PDK1, or pMIR-3′-UTR-E2F1 mutant, respectively (the underlines represent the mutated seed regions). (B) Nontargeted or *miR-9-3p* mimic was transfected into MCF-7 cells together with pMIR-3′-UTR-E2F1, pMIR-3′-UTR-E2F3, pMIR-3′-UTR-MDM2, pMIR-3′-UTR-PDK1, or pMIR-3′-UTR-E2F1 mutant and a control Renilla luciferase expression vector. 60 h after transfection, cells were harvested and assayed for relative luciferase units. (C) MCF-7 cells were transfected with nontargeted miRNA, *miR-9-3p* mimic, or *miR-9-3p* antagomir. 60 h after transfection, cells were harvested, and E2F1 expression was analyzed using RT-qPCR at the mRNA level (left) or Western blotting at the protein level (right). (D, top) MCF-7 cells were treated with PP242 or rapamycin as indicated and analyzed for E2F1 expression as described in C. (Bottom) 36 h after transfection with a *miR-9-3p* antagomir gradient, MCF-7 cells were treated with 200-nM PP242 for an additional 24 h, and E2F1 expression was analyzed via Western blotting. Error bars represent mean values ± SEM. ns, not significant.

dephosphorylation of c-Myc (Yeh et al., 2004), we further investigated whether mTORC2 dephosphorylates c-Myc at S62 through PP2A. Interestingly, knockdown of Rictor specifically reduced c-Myc–associated PP2A activity, but had little effect on global PP2A activity (Fig. 7 B). Furthermore, Rictor depletion or PP242 treatment significantly enhanced expression of CIP2A (cancerous inhibitor of PP2A; Fig. 7 A and Fig. S4, A–C), an endogenous inhibitor reported to suppress PP2A activity toward c-Myc S62 (Junttila et al., 2007). Moreover, Rictor coimmunoprecipitated with both PP2Ac (the catalytic subunit of PP2A;

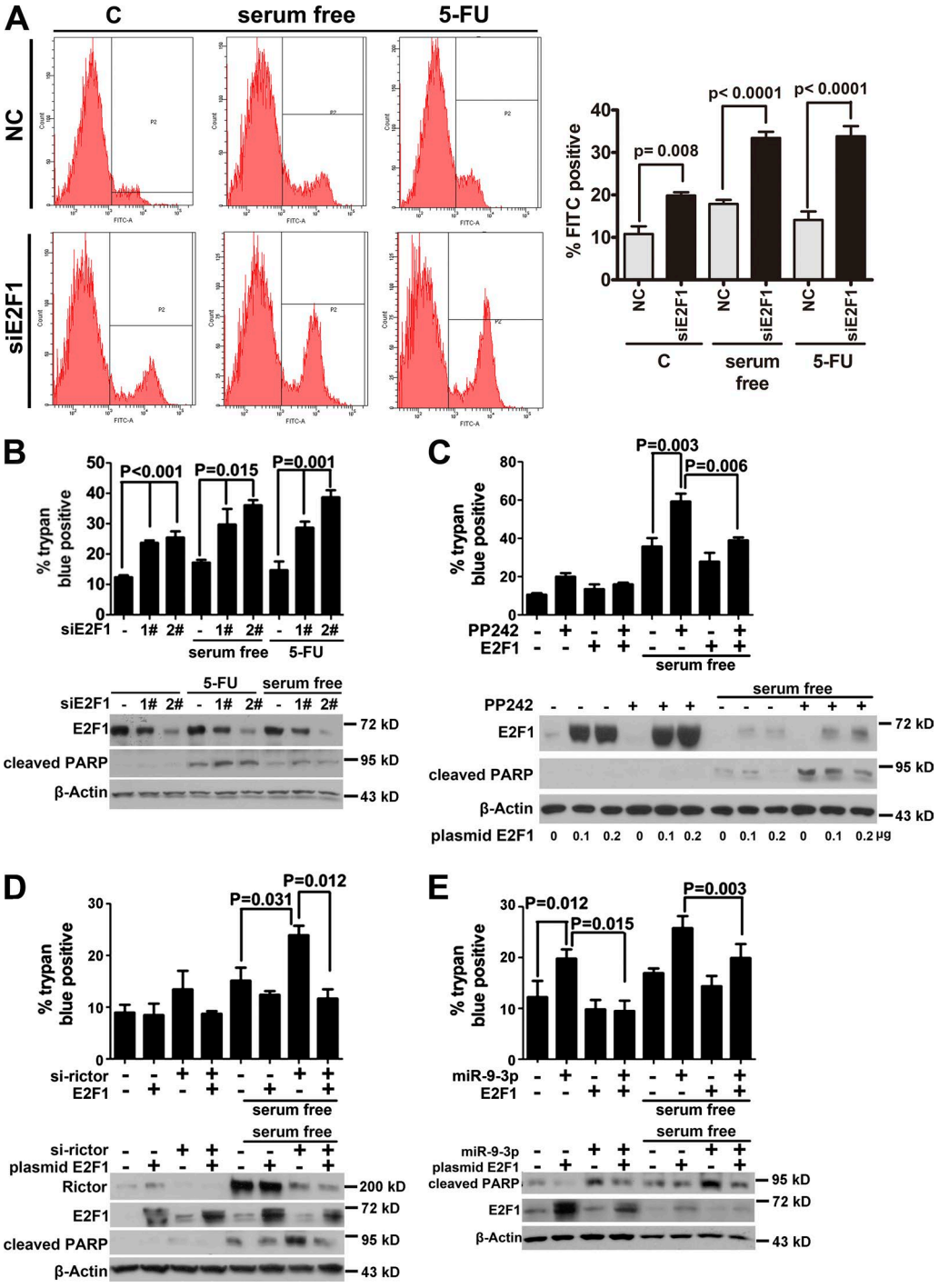


Figure 4. ***miR-9-3p* acts downstream of mTORC2 and triggers apoptosis by targeting E2F1.** (A) MCF-7 cells were transfected with a pool of two siRNAs (1:1) targeting different regions of E2F1 mRNA. After 36 h, cells were serum starved or treated with 400-µM 5-FU for an additional 24 h, harvested, and labeled with Annexin V–FITC and propidium iodide for analysis of apoptosis. The data shown are from a single representative experiment out of three repeats. (B) MCF-7 cells were transfected separately with the two siRNAs and treated as in A, followed by trypan blue staining (top) or Western blotting (bottom). (C) MCF-7 cells were transfected with vehicle or WT E2F1 in the absence or presence of PP242, as indicated. 12 h after transfection, cells were serum starved for an additional 24 h and harvested for either trypan blue staining (top) or Western blotting (bottom). (D) MCF-7 cells were sequentially transfected with Rictor siRNA and WT E2F1. After 24 h of serum starvation, the effects of ectopic E2F1 expression on Rictor knockdown were monitored via trypan blue staining (top) and Western blotting (bottom). (E) MCF-7 cells were sequentially transfected with *miR-9-3p* and E2F1, followed by assay as described in C. Error bars represent mean values ± SEM. C, control; NC, negative control.

Fig. 7 C and Fig. S4 D) and CIP2A (Fig. 7 C). Based on these results, we propose that Rictor interacts with both CIP2A and PP2A, promoting dephosphorylation of c-Myc at S62 by suppressing expression of CIP2A and activating PP2A. Interestingly, PP242 treatment induced binding of CIP2A with PP2Ac more significantly than up-regulation of CIP2A expression in the lysate (Fig. 7 D). Collectively, these results strongly suggest that mTORC2 serves to primarily down-regulate CIP2A present

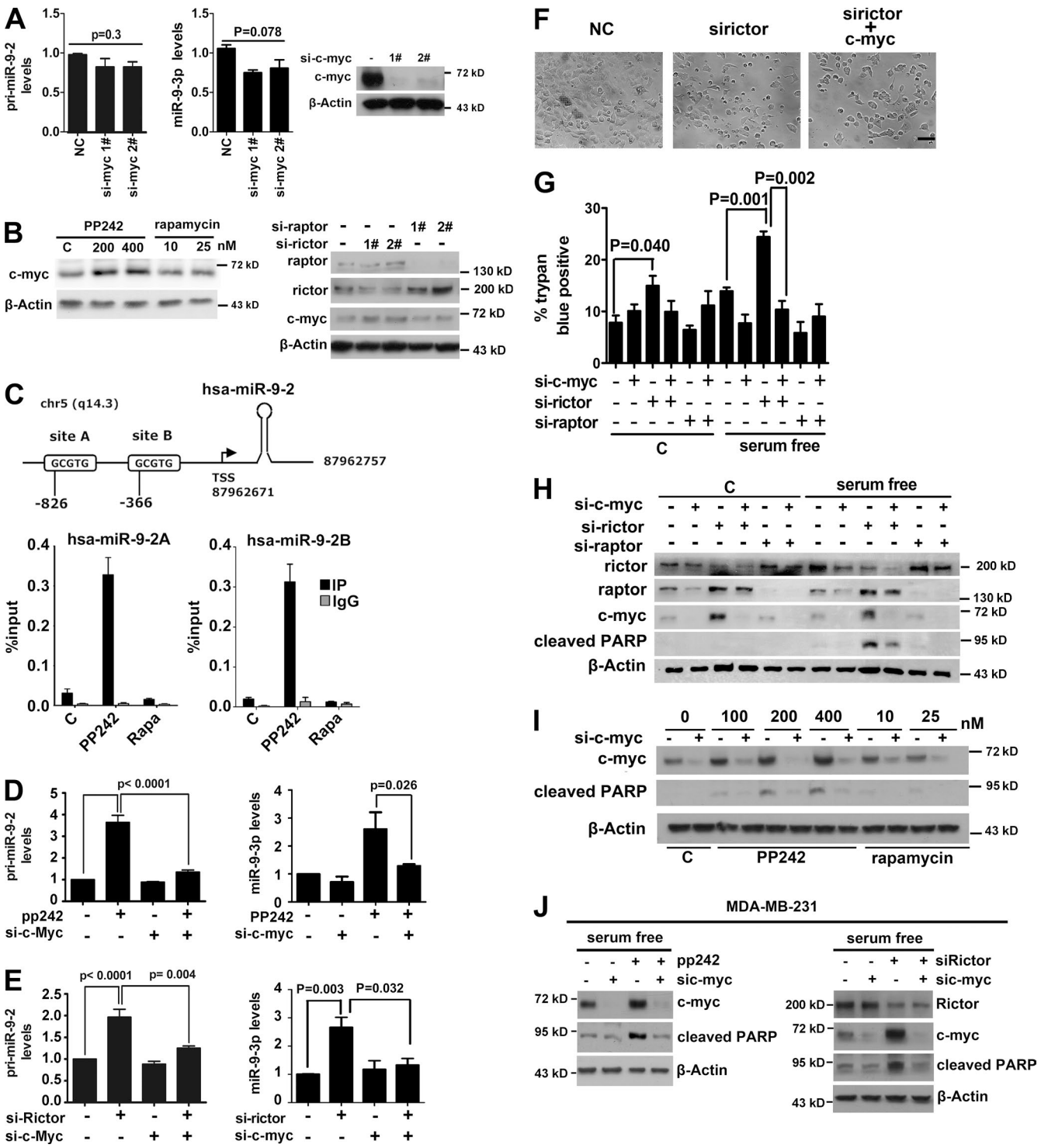


Figure 5. **mTORC2 mediates *pri-miR-9-2/miR-9-3p*/E2F1 signaling and apoptosis via c-Myc.** (A) The effect of silencing c-Myc on the *pri-miR-9-2/miR-9-3p* level was assayed using RT-qPCR (left and middle). Protein expression of c-Myc was analyzed via Western blotting (right). (B) MCF-7 cells were treated with PP242 or rapamycin (left) or transfected with two different siRNAs for Rictor and Raptor (right) as indicated, and their effects on c-Myc expression were monitored using Western blotting. (C) MCF-7 cells were treated with 200-nM PP242 or 10-nM rapamycin for 24 h and subjected to chromatin extraction. Sheared chromatin was immunoprecipitated with a c-Myc antibody and the two binding promoter regions of *hsa-miR-9-2* (one of three *miR-9-3p*–coding DNAs) augmented using RT-qPCR. (D and E) The effect of c-Myc silencing on the *pri-miR-9-2/miR-9-3p* level regulated by PP242 (D) or Rictor knockdown (E) was analyzed using RT-qPCR. (F–I) The effect of c-Myc silencing on apoptosis induced upon Rictor depletion or PP242 treatment was detected with a light microscope (F), trypan blue staining (G), or Western blotting (H and I), as indicated. Bar, 50 µm. (J) In MDA-MB-231 cells, the effect of c-Myc silencing on apoptosis induced upon 200-nM PP242 treatment (left) or Rictor depletion (right) was detected with Western blot analysis of PARP cleavage. C, control; NC, negative control; TSS, transcription start site. Error bars represent mean values ± SEM.

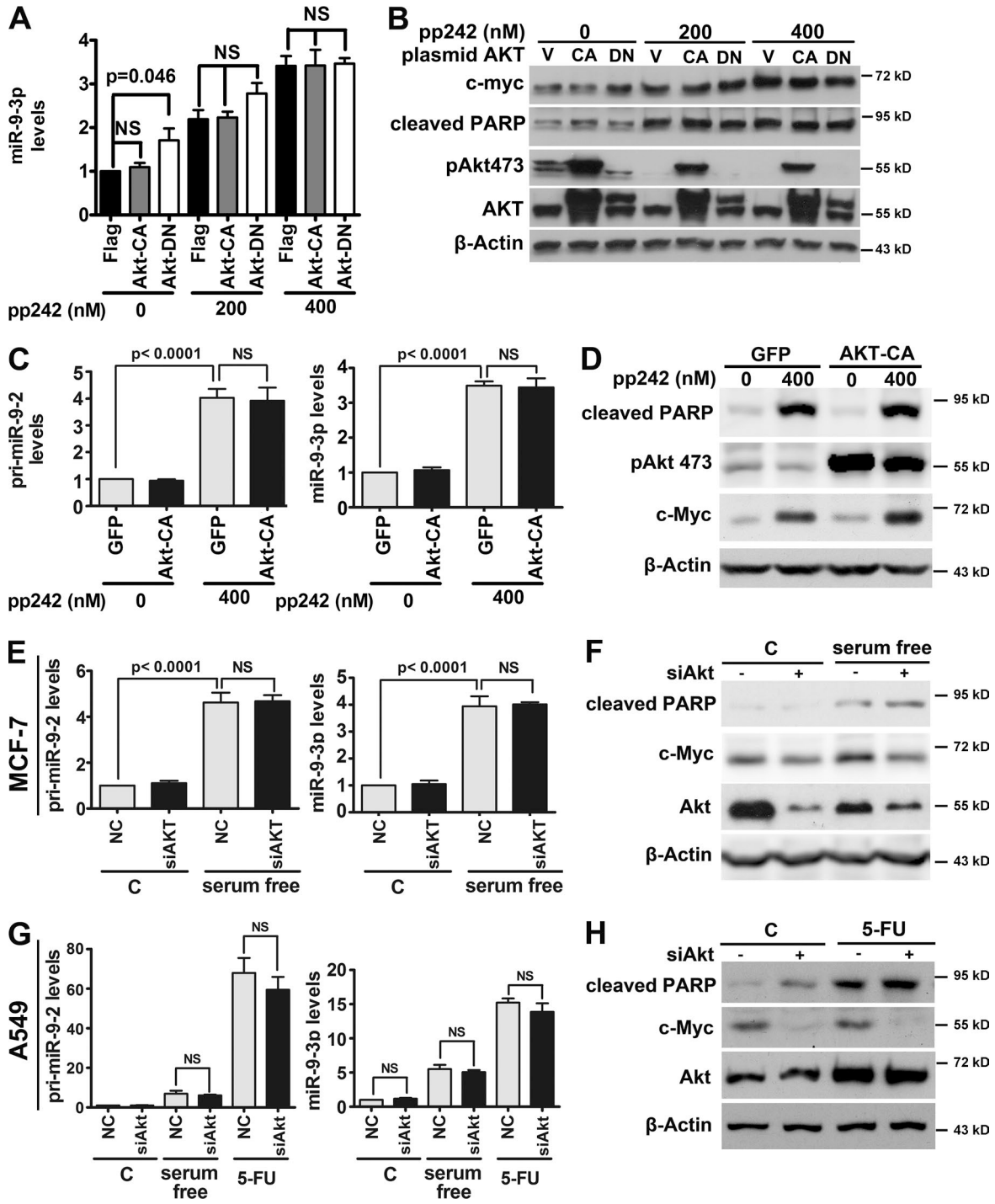


Figure 6. **mTORC2 suppresses c-Myc/*pri-miR-9-2*/*miR-9-3p* in an Akt-independent manner.** (A and B) MCF-7 cells were transfected with vector, pUSE-Akt CA, or pUSE-Akt DN, as indicated. 24 h after transfection, cells were treated with or without PP242 for an additional 24 h, harvested, and monitored to determine the *miR-9-3p* level using RT-qPCR (A) or analyzed for c-Myc expression and PARP cleavage using Western blotting (B). MCF-7 cells were cotransfected with pEGFP-N1 and pUSE-Akt CA (vector) and treated as in A, followed by FACS sorting. (C and D) Sorted cells were analyzed for *pri-miR-9-2*/*miR-9-3p* levels (C) or c-Myc expression and PARP cleavage (D). (E–H) MCF-7 (E and F) and A549 (G and H) cells were transfected with a pool of two different siRNAs of Akt1 (1:1). (E and G) 36 h after transfection, cells were serum starved or treated with 400-µM 5-FU for an additional 24 h and analyzed for *pri-miR-9-2* (left), *miR-9-3p* (middle), or c-Myc expression and PARP cleavage (F and H). Error bars represent mean values ± SEM. C, control; NC, negative control; V, vector.

in the CIP2A–PP2A–c-Myc complex, thereby inhibiting binding of CIP2A with PP2Ac. Thus, we propose that mTORC2 specifically promotes PP2A activity toward c-Myc S62 by blocking the binding of CIP2A with PP2Ac, although the exact mechanism has yet to be elucidated.

Global suppression of PP2A activity with a chemical inhibitor, okadaic acid (OA), or knockdown of PP2A catalytic subunit (PP2Ac) promoted S62 phosphorylation of c-Myc and subsequently up-regulation of *miR-9-3p* (Fig. 7 E). Conversely, global activation of PP2A using a chemical agonist,

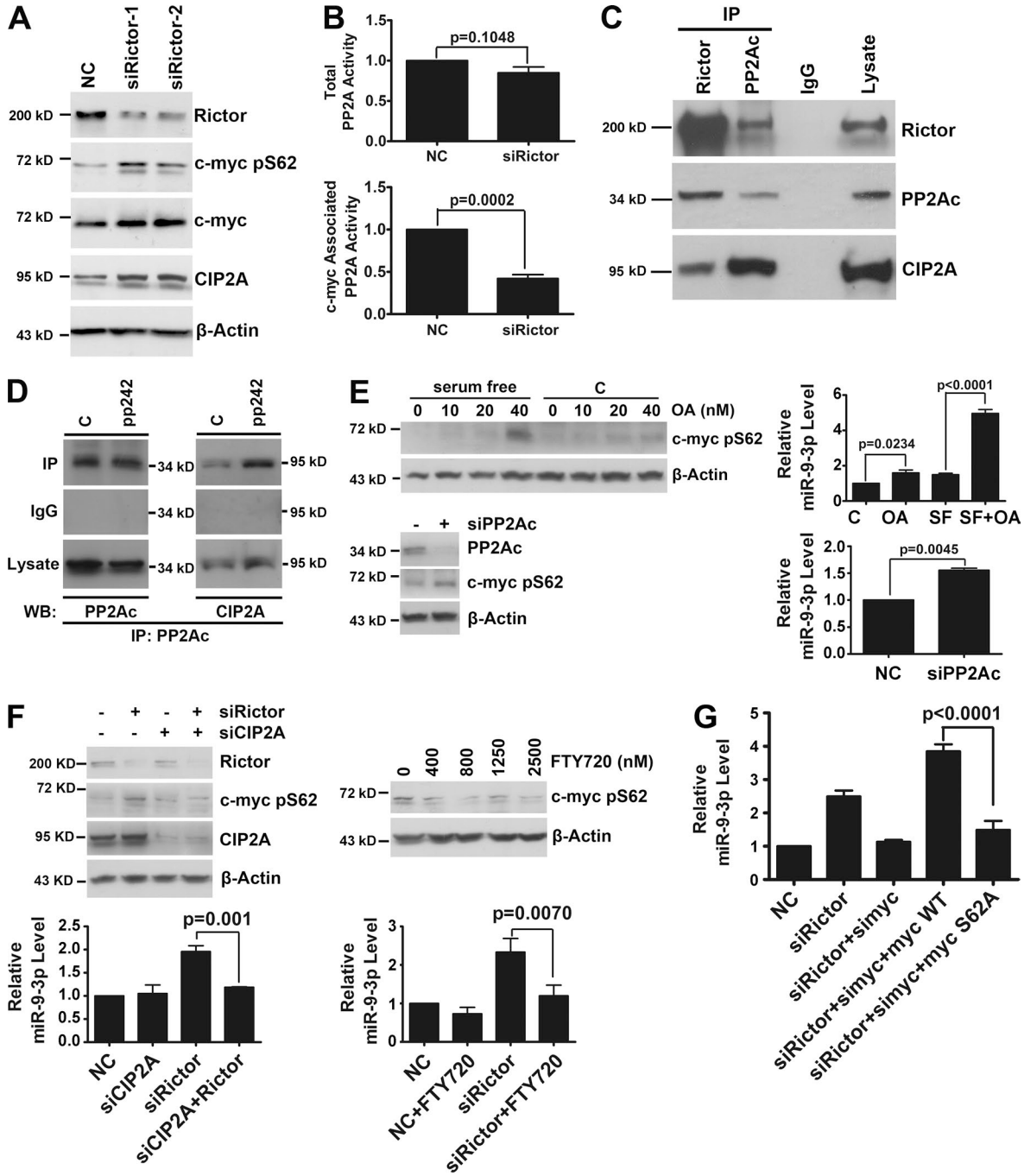


Figure 7. **mTORC2 suppresses c-Myc/*miR-9-3p* via PP2A-mediated dephosphorylation of c-Myc.** (A) MCF-7 cells were transfected with nontargeted siRNA (NC) or two siRNAs targeting different regions of Rictor mRNA. After 60 h, cells were harvested for Western blot analysis. (B) 60 h after transfection as indicated, MCF-7 cells were lysed and immunoprecipitated with PP2A (top) or c-Myc (bottom) and assayed for PP2A activity. For the latter, PP2A activity was normalized to immunoprecipitated c-Myc levels. (C) MCF-7 lysates were immunoprecipitated with antibodies against Rictor or PP2Ac and blotted for Rictor, PP2Ac, and CIP2A. (D) 200-nM PP242–treated MCF-7 cells were lysed, immunoprecipitated, and blotted as indicated. (E) MCF-7 cells were treated with OA gradient, as indicated, in the presence or absence of serum starvation for 24 h. After 24 h, cells were harvested for Western blotting (top left) or RT-qPCR analysis of *miR-9-3p* level (top right). MCF-7 cells were transfected with siRNA for PP2Ac (siPP2A). After 60 h, cells were harvested for Western blotting (bottom left) or RT-qPCR analysis of the *miR-9-3p* level (bottom right). (F) MCF-7 cells were cotransfected with siRNAs for both Rictor and CIP2A (left) or transfected with siRNA for Rictor followed by 2.5-µM FTY720 treatment for 24 h (right). 60 h after transfection, cells were harvested either for Western blot analysis (top) or RT-qPCR assay of *miR-9-3p* (bottom). (G) Effects of ectopic expression of WT c-Myc (myc WT) or S62A mutant (myc S62A) on the *miR-9-3p* level regulated by simultaneous silencing of Rictor and c-Myc were analyzed using RT-qPCR. Error bars represent mean values ± SEM. C, control; IP, immunoprecipitation; NC, negative control; SF, serum free; WB, Western blot.

FTY720, or specific activation of c-Myc–associated PP2A via simultaneous knockdown of CIP2A suppressed S62 phosphorylation of c-Myc and *miR-9-3p* up-regulated by Rictor silencing (Fig. 7 F). These results clearly confirm that mTORC2 suppresses c-Myc S62 phosphorylation and *miR-9-3p* expression through PP2A activity. Consistently,

ectopic reexpression of an S62A mutant of c-Myc (where serine at position 62 is mutated to alanine and cannot be phosphorylated) after simultaneous depletion of endogenous Rictor and c-Myc restored the *miR-9-3p* level to a markedly lower extent compared with its wild-type (WT) counterpart (Fig. 7 G), suggesting that S62 phosphorylation of c-Myc is critical for transcription of *miR-9-3p*. Our results collectively indicate that mTORC2 suppresses c-Myc/*miR-9-3p* through CIP2A/PP2A-mediated dephosphorylation of c-Myc at S62.

### Inhibition of mTORC2 modulates c-Myc–*miR-9-3p*–E2F1 to promote apoptosis in vivo

To validate the mechanism of mTORC2-mediated regulation of c-Myc–*miR-9-3p*–E2F1 in cell survival in vivo, two mouse models were used. First, nude mice bearing MDA-MB-231 breast tumor xenografts were treated with rapamycin or PP242. PP242 administration as a single agent markedly inhibited breast tumor growth (tumor areas and tumor weight), whereas rapamycin was ineffective in suppressing tumor growth (Fig. 8, A–C). In vivo administration of PP242, but not rapamycin, induced significant apoptosis in breast tumor xenografts, as observed from TUNEL assay (Fig. 8 D) and PARP cleavage data (Fig. 8 E, top). Western blot results revealed that PP242 suppresses both mTORC1 and mTORC2 in vivo, as evident from markedly reduced phosphorylation of Akt (Ser 473) and S6 (Ser 235/236), whereas rapamycin suppresses only mTORC1, based on the significant reduction of phosphorylation of S6, but not Akt (Fig. 8 E, bottom). The *miR-9-3p* level was up-regulated (Fig. 8 F) while E2F1 was simultaneously down-regulated in tumor xenografts administered with PP242, but not rapamycin (Fig. 8 E).

Lymphocytes undergo spontaneous apoptosis to prevent the autoimmune response, which requires expression of endogenous c-Myc (Shi et al., 1992). An earlier investigation has reported an Eμ-Myc transgenic mouse model displaying significant apoptosis in the B cell compartment (Jacobsen et al., 1994). Another recent study showed that Rictor is crucial for B lymphocyte survival (Lee et al., 2013). Considering these findings, B lymphocytes may be the perfect model for studying c-Myc–mediated apoptosis under conditions of mTORC2 deactivation. Thus, to examine the roles of c-Myc/*miR-9-3p* and E2F1 in mTORC2-mediated B cell survival, we generated mice with a conditionally ablated Rictor gene in B lymphocytes (B cell–Rictor knockout [KO]) using a Cre expression cassette under control of the CD19 promoter (Fig. S5 A). Although conventional Rictor-KO mice died at the embryonic stages, B cell–Rictor KO mice were born with normal Mendelian ratios and grew normally (Fig. S5 B). As expected, Rictor was only observed in B lymphocytes isolated from the spleens of WT littermates, but not those of KO mice (Fig. S5 C), suggesting that Cre recombination of the floxed Rictor gene is completed after birth. Rictor deficiency in B lymphocytes led to reduced splenic B cell number (Fig. S5 D) and enhanced apoptosis (Fig. 8, G, H, and J). Importantly, c-Myc and *miR-9-3p* levels were up-regulated, and, consequently, E2F1 was down-regulated in B lymphocytes of B cell–Rictor KO compared with WT mice (Fig. 8, I and J).

### *Antagomir-9-3p* reverses mTORC1/2 inhibitor–potentiated apoptosis and growth inhibition in xenograft tumors

The findings shown in Fig. 8 demonstrate that mTORC2 inhibition induces *miR-9-3p* expression and cell death in vivo. To further validate that mTORC2 inhibition potentiates cell apoptosis through *miR-9-3p*, a rescue experiment was performed in vivo. Intratumoral injection of *antagomir-9-3p* in MDA-MB-231 breast tumor xenografts significantly reversed the effect of AZD8055 (a novel kinase inhibitor of mTORC1/2) on cell growth, as evident from the tumor growth curve (Fig. 9 A) and final tumor weight (Fig. 9 B). Notably, *antagomir-9-3p* dramatically suppressed apoptosis induced by AZD8055, determined based on the significant reduction in PARP cleavage (Fig. 9 C) and TUNEL labeling (Fig. 9 D). Consistently, treatment with *antagomir-9-3p* induced recovery of E2F1 protein expression down-regulated by AZD8055, even with augmented CIP2A/c-Myc expression (Fig. 9 C).

These in vivo data validate the findings that down-regulation of CIP2A/c-Myc and *miR-9-3p* and up-regulation of E2F1 constitute part of the critical mechanism underlying mTORC2-modulated cell survival. A schematic representation of the pathway is shown in Fig. 9 E.

## Discussion

Extensive studies have shown that miRNAs exert their functions in cancer progression through targeting the mTORC1/2 signaling pathway (Uesugi et al., 2011; AlQurashi et al., 2013; Jin et al., 2013). However, limited information is available on whether miRNAs play a role in the control of cell growth, proliferation, and survival by mTORC1/2 in response to growth factors, energy, stress, and nutrients. Rapamycin has been shown to up-regulate or down-regulate specific miRNAs, which play critical roles in muscle cell differentiation during skeletal myogenesis or rapamycin resistance in cancer therapy (Sun et al., 2010; Totary-Jain and Marks, 2013; Totary-Jain et al., 2013; Trindade et al., 2013). To date, the miRNAs specifically regulated by mTORC2 remain to be identified. Our experiments revealed eight miRNAs that were specifically modulated by mTORC2, but not mTORC1, including *miR-9-3p*. Moreover, mTORC2 promoted cell survival via inhibition of *miR-9-3p* and up-regulation of E2F1 in a PP2A–c-Myc–dependent manner. Our results collectively suggest that mTORC2 inhibition or depletion stimulates the expression of *miR-9-3p*, which directly targets E2F1 to promote genotoxic drug–induced apoptosis, thus revealing a novel mechanism for cell survival control by mTORC2-regulated miRNAs. Differential regulation of miRNAs by mTORC1 and mTORC2 may also explain why mTOR kinase inhibitors are more effective than rapalogs for cancer treatment. Rapamycin may up-regulate prosurvival miRNAs and down-regulate proapoptotic miRNAs, which contribute to rapamycin resistance in cancer therapy (Totary-Jain and Marks, 2013; Totary-Jain et al., 2013). Our findings provide evidence that targeting mTORC2 has promising therapeutic benefits for overcoming genotoxic drug resistance through induction of proapoptotic *miR-9-3p*. Further in vivo studies are required to clarify the specific roles and mechanisms of *miR-9-3p* in enhancing the chemotherapeutic effects of mTOR inhibitors and genotoxic drugs.

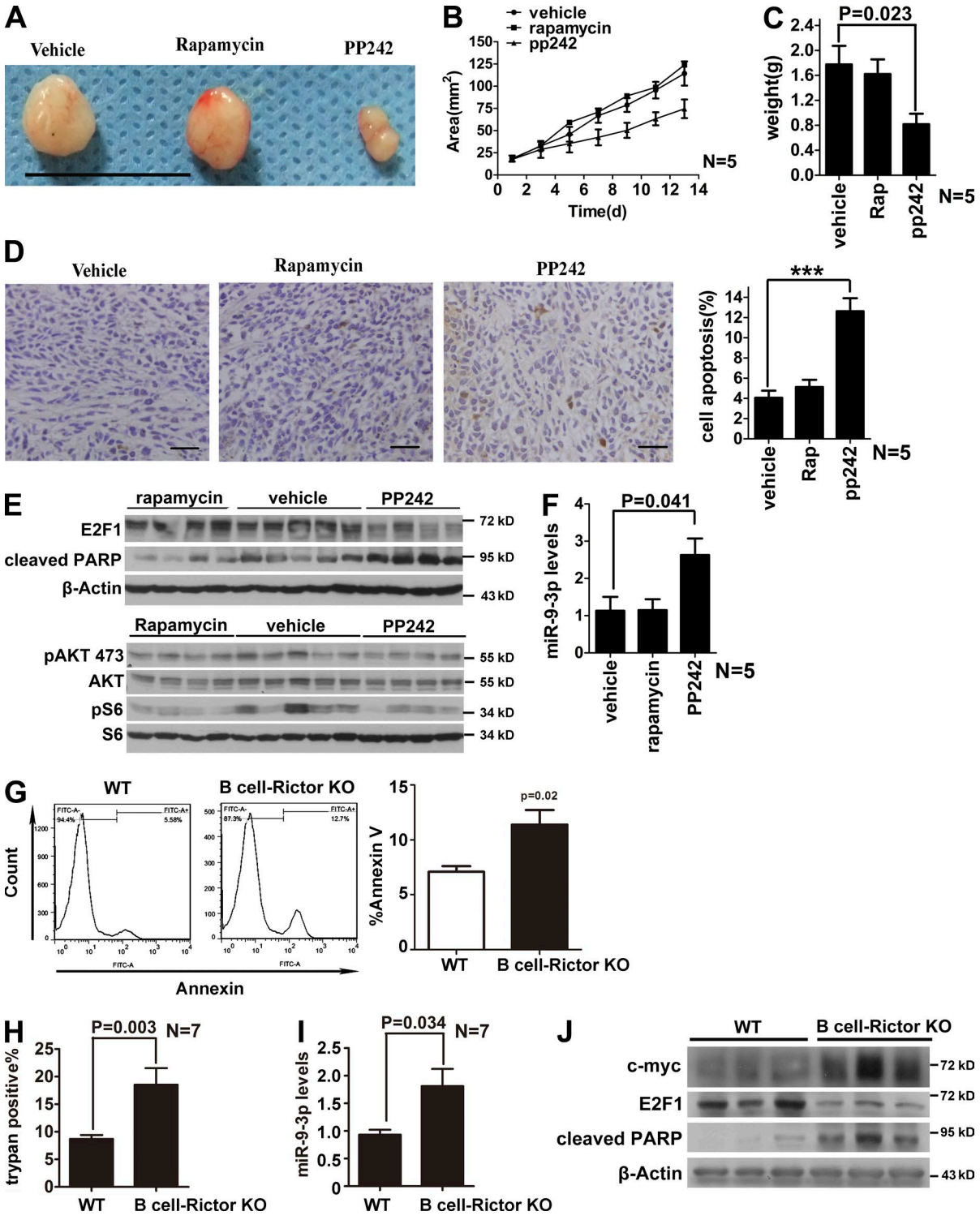


Figure 8. **mTORC2 modulates c-Myc/*miR-9-3p*/E2F1 to promote survival in tumor xenografts and a mouse genetic model.** (A and B) Images (A) and tumor growth curves (B) of MDA-MB-231 xenografts in BALB/c nude mice treated with vehicle, rapamycin, or PP242 daily by gavage. Treatment groups comprised five mice each. Each data point signifies the estimated tumor areas. Bar, 1 in. (C) Tumor weights of MDA-MB-231 xenografts in nude mice treated with vehicle, rapamycin, or PP242. (D) MDA-MB-231 xenografts were subjected to TUNEL labeling, with the percentage of apoptotic cells calculated under a light microscope. ***, $P < 0.001$ for comparison of PP242 therapy versus control therapy. Bars, 50 µm. (E and F) MDA-MB-231 xenografts were analyzed for expression of the indicated proteins via Western blotting (E) or *miR-9-3p* via RT-qPCR (F). (G–J) B lymphocytes from mice conditionally deficient in the Rictor gene were harvested and analyzed for cell death rate with Annexin V labeling (G) and trypan blue staining (H), expression of *miR-9-3p* with RT-qPCR (I), or cleavage of PARP and expression of c-Myc and E2F1 using Western blotting (J). The figures shown are from a single representative experiment out of three repeats. Error bars represent mean values ± SEM.

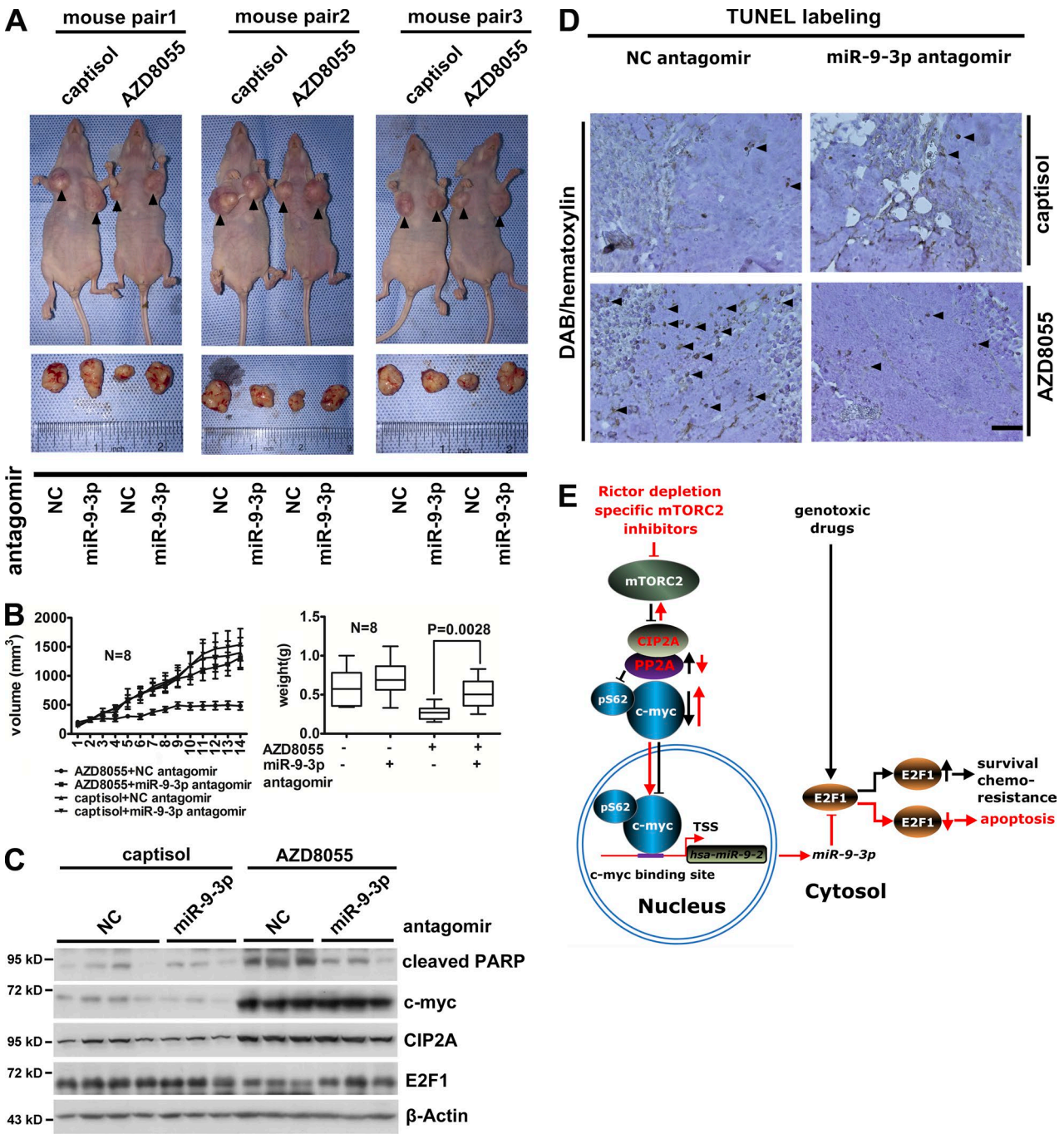


Figure 9. ***Antagomir-9-3p* restores AZD8055-suppressed growth and survival of tumor xenografts.** (A and B) BALB/c nude mice were treated with captisol or AZD8055 by gavage and intratumorally injected with antagomirs of NC and *miR-9-3p*. Each treatment group comprised eight mice. (A) Representative images of mice (top) and MDA-MB-231 xenografts (bottom). (B) Tumor growth curves (left) and tumor weights (right) of MDA-MB-231 xenografts. (C and D) MDA-MB-231 xenografts treated as described in A were either analyzed for the indicated proteins by Western blotting (C) or subjected to TUNEL labeling (D). Images of DAB/hematoxylin staining under a light microscope (40×) are shown. Bar, 50 µm. Arrowheads indicate apoptotic cells. (E) A schematic diagram illustrates the currently defined mTORC2–CIP2A–PP2A–c-Myc–*miR-9-3p*–E2F1 pathway. Error bars represent mean values ± SEM. NC, negative control.

As *miR-9-3p* and its nonstar counterpart *miR-9-5p* exert opposite functions (death vs. survival), despite being encoded by the same genes and spliced from the same precursor, it would be interesting to elucidate whether these two miRNAs are simultaneously activated and deactivated, or one activated and the other deactivated under certain conditions. Our experiments demonstrated that *miR-9-3p* is significantly up-regulated upon Rictor depletion, whereas expression of *miR-9-5p* is slightly suppressed (Fig. S2 B), supporting the theory that these two companion miRNAs are orchestrated to fine-tune cell fate. mTORC1 has been shown to induce the degradation of Ago2 in T cells (Bronevetsky et al., 2013), a pivotal factor exhibiting preference for miRNA "star" strand selection in *Drosophila* (Okamura et al., 2009). Hence, the possibility that mTORC2 suppresses the expression of *miR-9-3p*, not only at the transcriptional but also the posttranscriptional level via modulating certain types of

Argonautes, and thus alters strand selection preference toward *miR-9-3p*/*5p* cannot be excluded. Further studies are required to establish the relationship between both mTORCs and different types of Argonautes with the aim of clarifying the posttranscriptional regulatory mechanism of mTORC2 action on *miR-9-3p*.

Although Akt is the only established substrate of mTORC2 known to promote cell survival (Oh and Jacinto, 2011), recent studies have additionally reported that Akt down-regulates c-Myc and inhibits c-Myc–dependent apoptosis (Rohn et al., 1998; Gill et al., 2013; Yeh et al., 2013). Consistently, our results showed that inhibition of Akt via ectopic expression of AKT-DN induces a moderate increase in c-Myc and *miR-9-3p* expression, indicating a possible role of Akt in preventing c-Myc–*miR-9-3p* activation. Nevertheless, reactivation of Akt failed to suppress c-Myc–*pri-miR-9-2–miR-9-3p* and corresponding apoptosis induced by mTORC2 inhibition, and silencing endogenous Akt did not further increase c-Myc–*pri-miR-9-2–miR-9-3p* levels triggered by serum starvation and 5-FU treatment, suggesting that tumor cells initiate the c-Myc–*pri-miR-9-2–miR-9-3p*–E2F1 apoptotic pathway via a mechanism bypassing control of Akt under these conditions. Remarkably, Rictor depletion or PP242 treatment induced up-regulation of CIP2A and binding to PP2Ac to a more significant extent, reducing PP2A phosphatase activity toward c-Myc S62, leading to enhanced S62 phosphorylation of c-Myc, and consequent stabilization of c-Myc and transcription of *miR-9-3p*. Mechanistically, Rictor interacts with both CIP2A and PP2Ac. Notably, deletion of CIP2A or reactivation of PP2A reversed the induction of proapoptotic *miR-9-3p* upon mTORC2 inhibition, suggesting that these two proteins are novel targets of mTORC2 that play important roles in mTORC2-mediated survival. The mTORC2–CIP2A–PP2A cascade may represent a novel Akt-independent mechanism by which mTORC2 mediates c-Myc–*pri-miR-9-2–miR-9-3p*–E2F1 and promotes tumor cell survival. Although mTORC2 promotes tumor cell survival via both the CIP2A–PP2A–c-Myc–*pri-miR-9-2–miR-9-3p*–E2F1 cascade and Akt in the physiological state, loss of mTORC2 activity possibly reprograms the signaling network and renders tumor cells susceptible to the c-Myc–*miR-9-3p* apoptotic pathway, even when Akt activity is sufficiently high. The findings of this study are of particular interest in view of multiple lines of evidence showing that Akt activity is pivotal in primary drug resistance (Clark et al., 2002; Knuefermann et al., 2003; Pei et al., 2009) and acquired resistance conferred by chemotherapy (Huang and Hung, 2009) and provide novel mechanistic insights to facilitate effective combination therapy with agents targeting mTORC2 and genotoxic drugs for eliminating drug resistance.

E2F1 has been identified as a key regulator of apoptosis. However, recent evidence indicates that activated E2F1 plays an unexpected prosurvival role and represents a mechanism for cancer drug resistance in association with tumor progression (Stanelle and Pützer, 2006; Pützer and Engelmann, 2013). Although EGF receptor–Ras–Raf–MAPK, PI3-K–Akt, and NF-κB pathways have been identified as targets of E2F1 for promoting cell survival (Ladu et al., 2008; Zheng et al., 2009), the mechanism underlying survival signaling that antagonizes drug-induced cell death remains poorly defined and is possibly highly redundant. There is an urgent need to develop effective strategies for reducing E2F1 expression and activity to overcome drug resistance. As shown here, down-regulation of E2F1 and promotion of DNA damage–induced apoptosis via targeting mTORC2 provides a potential strategy to overcome E2F1-related drug resistance. Furthermore, regulation of E2F1 represents a previously unknown mechanism through which mTORC2 promotes cell survival and cancer progression.

Using cellular and mouse genetic models, we demonstrated that mTORC2 negatively regulates *miR-9-3p* to enhance E2F1 expression and promote cell survival in a CIP2A–PP2A–c-Myc–dependent manner. c-Myc, initially documented for its role in promoting cell cycle progression, is now recognized as a double-edged sword in malignancy because it is the most robust agent encoded in our genome, both to promote proliferation and trigger cell death (McMahon, 2014). Although normal cells with high-level ectopic expression of c-Myc often undergo apoptosis (Wyllie et al., 1987; Askew et al., 1991; Neiman et al., 1991), tumor cells have acquired the ability to resist the death-inducing effects of elevated endogenous c-Myc. One of the most well-characterized mechanisms gained by tumor cells to antagonize the apoptotic effects of c-Myc through evolution is parallel BCL-2 activation (Letai et al., 2004; Ozdek et al., 2004), which can blunt the c-Myc–initiated death pathway in a mitochondria-dependent manner. The signaling events preventing c-Myc activation to exert apoptosis, but not otherwise initiating a compensatory pathway to counterbalance its death-inducing effect, have been elucidated to a limited extent so far. Our results clearly suggest that mTORC2 serves as a pivotal signaling intersection point switching the c-Myc–*miR-9-3p* apoptotic pathway on or off. With the present findings, our knowledge of mTORC2 as a key signaling rheostat in cell growth and survival has expanded further. Sophisticated control of the CIP2A–PP2A–c-Myc axis by mTORC2 may also aid in alleviating the controversy with regard to the c-Myc switch toward transformation/proliferation or apoptosis. When activity of mTORC2 is high, CIP2A–PP2A–c-Myc mainly functions to promote transformation/proliferation, and when activity is low, apoptosis may be triggered through induction of *miR-9-3p* and suppression of E2F1. From this point of view, simply deactivating the CIP2A–PP2A–c-Myc axis (such as using new inhibitory compounds directly targeting c-Myc) may not represent the most effective tumor treatment strategy, as this may cause unanticipated side effects by blocking the proapoptotic potential of c-Myc. Additionally, the best-characterized apoptotic effect of c-Myc is associated with p53 (Zindy et al., 1998). However, p53 mutates and loses its function in about half of all human malignancies. Moreover, mutant p53 counterattacks to promote cancer cell survival (Engelmann and Pützer, 2012; Pützer and Engelmann, 2013). Therefore, the currently discovered CIP2A–c-Myc–*miR-9-3p*–E2F1 pathway represents an alternative way to initiate apoptosis in these tumors with p53 mutations. Most importantly, in conjunction with our results from human cancer cell lines with WT p53 (MCF-7 and A549) or mutant p53 (MDA-MB-231, PC-3M, and HCT116), mouse xenografts, and a mouse genetic model, our current findings suggest that this pathway represents a general proapoptotic mechanism in tumors, even if p53 is mutated. Not surprisingly, as E2F1 is primarily responsible for trans-activation of mutant p53 (Engelmann and Pützer, 2012; Pützer and Engelmann, 2013; Muller and Vousden, 2014), initiating this pathway will probably carry out its proapoptotic functions also by suppressing the transcription of mutant p53.

Our results collectively highlight a novel mechanism for cell survival control by mTORC2 and further support the utility

of targeted mTORC2 inhibition as a potential strategy, not only to recover the apoptotic potential of endogenous c-Myc–*miR-9-3p* but also to overcome E2F1-related drug resistance. It also provides a new rationale for simultaneously administrating *miR-9-3p* when issuing genotoxic drug treatment, which may help to eliminate or at least mitigate chemoresistance caused by E2F1 induction.

## Materials and methods

### Chemicals and reagents

Rapamycin, pp242, and 5-FU were purchased from Sigma-Aldrich. AZD8055 was obtained from Active Biochem. TRIzol reagent, Lipofectamine 2000, and Opti-MEM were acquired from Invitrogen. FTY720 (fingolimod) was obtained from Selleck. OA was purchased from Beyotime. The Dual-Luciferase Reporter Assay kit was acquired from Promega, and the ChIP-IT Express Enzymatic Chromatin Immunoprecipitation kit from Active Motif. The PP2A Immunoprecipitation Phosphatase Assay kit was purchased from EMD Millipore. The Hairpin-it microRNA and U6 snRNA Normalization RT-PCR Quantitation kit was acquired from GenePharma. The High Sensitive MiRNA Northern Blot Assay kit was obtained from Signosis. The In Situ Cell Death Detection kit was purchased from Roche. Among the antibodies used for immunoblotting, immunoprecipitation, and chromatin immunoprecipitation (ChIP), mouse monoclonal antibodies against PP2A and E2F1 were purchased from EMD Millipore; mouse monoclonal antibody against S6 and goat polyclonal antibody against AKT, all HRP-conjugated secondary antibodies, and Western Blotting Luminol Reagent were acquired from Santa Cruz Biotechnology,Inc.; and rabbit polyclonal antibodies targeting Rictor, c-Myc, CIP2A, PARP, phosphorylated S6 at Ser 235/236, and phosphorylated AKT at Ser 473 were procured from Cell Signaling Technology. Rabbit polyclonal antibody targeting c-Myc specifically phosphorylated at S62 was obtained from Abcam.

### Cell culture

MCF-7, MDA-MB-231, PC-3M, HEK293, and A549 cells were obtained from ATCC, and HCT116 was a gift from David J. Kwiatkowski (Brigham and Women's Hospital, Boston, MA). All cells were maintained according to the protocols of ATCC.

### Microscopy and image analyses

Cells were visualized with a 40×/0.55 (dry lens) objective using an inverted microscope (DIAPHOT 200; Nikon) at RT. Images were then captured with a digital camera (DS-Fi1; Nikon) using the autoexposure settings of NIS Elements BR 3.0 software (Nikon). For monitoring xenograft sections, bright field microscopy was performed at RT using a microscope (Eclipse 50i; Nikon) equipped with a Plan Fluor 20×/0.50 NA or 40×/0.75 NA objective lens (Nikon), a camera (VisiCam 3.0; VWR International), and VisiCam Image Analyzer software (VWR International). No imaging medium was used. After image acquisition, the images were color corrected using the match color command in Photoshop (CS 6.0; Adobe) to normalize for some exposure and lighting variations if the images for comparison were significantly different. This adjustment was applied to every pixel in each image.

### Xenograft experiments and intratumoral injection

MDA-MB-231 cells ($10^6$/injection) were injected subcutaneously into 6-wk-old BALB/c nude mice. After 7 d, mice were randomized into three groups ($n = 5$) and treated each day with vehicle control, 1 mg/kg rapamycin, or 10 mg/kg PP242 dissolved in water containing 5% 1-methyl-2-pyrrolidinone and 15% polyvinylpyrrolidone. For rescue experiments in vivo (*AntagomiR-9-3p* intratumoral injection), MDA-MB-231 cells were injected subcutaneously into the left and right armpits of the mice. 7 d later, mice were randomized into two groups ($n = 8$) and treated daily with 30% Captisol (wt/vol) or AZD8055 dissolved in 30% Captisol (20 mg/kg) by gavage. To minimize individual differences between mice, *AntagomirNC* and *Antagomir-9-3p* (10 µg/tumor) was directly injected into tumors in the right and left armpits of each mouse, respectively, every 3 d. Bidimensional tumor measurements were obtained every other day until sacrifice 14 d after the first gavage. Tumor diameters were measured with a caliper. Tumor volume ($V$) was calculated using the formula $V = ab^2/2$, whereby $a$ indicates length (millimeter) and $b$ indicates breadth (millimeter). Tumors were removed, weighed, and subjected to either Western blotting, RT-qPCR, or TUNEL analysis.

### siRNAs, mimics, and antagomirs of miRNAs and plasmid transfections

Cells were transfected with siRNAs, miRNAs, and plasmids using Lipofectamine 2000 according to the manufacturer's instructions. The siRNA sequences are listed in Table S3. Unless otherwise indicated in the figure legends, the siRNAs used for Rictor and Raptor were Rictor-1 and Raptor-1, respectively (Table S3). The typical concentration of siRNA and miRNA was 40 nM, and that of plasmids was 1 µg/ml. For the E2F1 plasmid, only 0.2 µg was transfected into 1 well of a 24-well plate because of its ultra-high expression. Upon transfection of c-Myc siRNAs, both strands were pooled (at a 1:1 ratio). All miRNA mimics and antagomirs were designed and synthesized by GenePharma and are listed in Table S3. Plasmids pUSE-Akt-WT (21-153), pUSE-Akt-CA (21-151), and pUSE-Akt-DN (21-152) were obtained from EMD Millipore. They code for mouse Akt1 (WT), mouse Akt1 with N-terminal myristoylation, or mouse Akt1 (K179M mutant) fused to Myc-His under cytomegalovirus promoter, respectively. Plasmid myc-Rictor (plasmid 1860; Sarbassov et al., 2004) coding for human Rictor fused to Myc in pRK-5 and plasmid pSG5L HA E2F1 (plasmid 10736; Sellers et al., 1998) coding for human E2F1 fused to HA in pSG5L were obtained from Addgene. Plasmid pD40-His–c-Myc coding for human WT c-Myc fused to His and pD40-His–c-Myc$^{S62A}$ coding for human c-Myc mutant (S62A) fused to His in pDEST-40 mammalian expression vector were gifts from Rosalie Sears (Molecular and Medical Genetics, Oregon Health and Sciences University, Portland, OR).

### miRNA microarray, RNA isolation, and RT-qPCR

Total RNA was extracted from MCF-7 cells using TRIzol reagent according to the manufacturer's instructions, with the following modifications: the isopropanol precipitation step was elongated to overnight at −20°C, and the concentration of washing ethanol increased to 80%. Although RT-qPCR for *miR-9-3p* was conducted according to the manual of Hairpin-it microRNA and U6 snRNA Normalization RT-PCR Quantitation kit, RT-qPCR for *hsa-pri-miR-9-1*, *hsa-pri-miR-9-2*, *and hsa-pri-miR-9-3* was conducted according to the instructions of TaqMan Pri-miRNA Assays (Applied Biosystems) after total RNA extraction and purification with TURBO DNA-free kit (Ambion). For miRNA array assay, samples were submitted to Shanghai Biotechnology Corporation for hybridization on an Agilent human miRNA array (version 12.0). Each microarray chip was hybridized to a single sample labeled with Cy3. Background subtraction and normalization were performed. Finally, miRNAs with expression levels differing by at least threefold between control and PP242 (or rapamycin)-treated cells were selected ($P < 0.05$). Whole miRNA array datasets are available in the GEO database under accession no. GSE61289.

### Algorithm tools to predict targets of *miR-9-3p*

PicTAR (New York University Center for Genomics and Systems Biology; and Max Delbruck Center for Molecular Medicine), TargetScan (Whitehead Institute for Biomedical Research), and microRNA (Memorial Sloan Kettering Cancer Center) were applied to predict the potential targets of *miR-9-3p*. Only targets predicted using all three tools were sorted and categorized. Putative targets related to apoptosis and closely correlated with mTOR were further subjected to the luciferase verification system.

### PP2A activity assay

In brief, cells were suspended in lysis buffer (50-mM Tris-HCl, pH 7.4, 7.5% glycerol, 1-mM EDTA, 150-mM NaCl, 0.5% NP-40, 1-mM $Na_3VO_4$, and cOmplete Protease Inhibitor [Roche]), cleared of debris via centrifugation for 15 min at 12,000 rpm, and incubated with PP2A or c-Myc antibody, followed by protein A agarose beads provided in the kit. After washing, the beads were resuspended in a mixture of PP2A phosphatase reaction buffer and threonine phosphopeptide and incubated for 10 min at 30°C in a shaking incubator, followed by detection of released phosphate with Malachite green solution.

### ChIP assay

ChIP was performed on chromatin isolated from ∼2 × $10^6$ cells using the ChIP-IT Express Enzymatic Chromatin Immunoprecipitation kit (Active Motif) according to the manufacturer's protocol. RT-qPCR of coimmunoprecipitated genomic DNA fragments was performed with the promoter-specific primers listed in Table S2.

### Northern blot assay

Northern blotting was performed according to the instructions of the High Sensitive MiRNA Northern Blot Assay kit user manual (Signosis). In brief, total RNA was extracted with TRIzol reagent and quantified using a spectrophotometer (NanoDrop; Thermo Fisher Scientific). A 7-µl aliquot of total RNA (15 µg) was mixed with 3 µl gel loading buffer, denatured at 70°C for 5 min, and loaded onto a 15% TBE-urea gel. Gels were run, and the separated RNAs were transferred to the membrane, cross-linked via UV, and hybridized to a highly sensitive biotin-labeled miR-9-3p probe customized by Signosis. After amplification, the target miRNA–probe complex was incubated with streptavidin–horseradish peroxidase conjugate and detected via chemiluminescence.

### Luciferase reporter assay

The 3′ UTR sequences containing the predicted binding sites for *miR-9-3p* of E2F1, E2F3, MDM2, and PDK1 were cloned into pMIR-REPORT (Ambion) downstream of Firefly luciferase, with a short extension containing cleavage sites for SpeI (5′ end) and MulI (3′ end). The resultant reporter gene constructs were transfected into MCF-7 cells with a *miR-9-3p* mimic, together with an internal control plasmid, pGL4.74[hRluc/TK] (Promega). 24–48 h after transfection, cells were lysed, and Firefly/Renilla luciferase activities were measured using the Dual-Luciferase Reporter Assay System. To further confirm targeting of E2F1 mRNA by *miR-9-3p*, mutant constructs of 3′ UTR-E2F1 were synthesized (for sequences, see Tables S4 and S5) and cloned into pMIR-REPORT. MCF-7 cells were similarly transfected with the WT or M reporter, and Firefly/Renilla luciferase activities were measured the same way. WT and mutant primers are listed in Table S4.

### Generation of B cell–specific *Rictor* deletion mice

All animal experiments were performed with the approval of the Southern Medical University Animal Care and Use Committee in accordance with the guidelines for the ethical treatment of animals. *Cd19-Cre* mice (C57BL/6 background) with a Cre recombinase gene inserted into the first coding exon of the CD19 antigen gene were obtained from The Jackson Laboratory. *Rictor* floxp mice were provided by Mark A. Magnuson (Vanderbilt University, Nashville, TN). In brief, a 9.9-kb DNA fragment, containing sequences from 7.5 kb upstream to 2.3 kb downstream of *rictor* exon 3, served as the starting point for insertion of the recombinase recognition sites. The loxP sites flanking exon 3 are located 283 bp upstream and 198 bp downstream of the exon. We crossbred floxp mice with Cre mice to generate Cre-flox/flox mice and flox/flox littermate controls. PCR analyses of genomic DNA from mouse tails were performed to determine genotype using the primers described in Table S4.

### Flow cytometry

B cell subpopulations in the spleen were defined as described previously (Walker et al., 1979). Transitional B cells were $B220^+CD93^+IgM^+$, follicular B cells were $B220^+CD^{23+}IgD^{high}IgM^{low}$, and marginal zone B cells were $B220^+CD23^{low}CD21^{high}$. Trans B was gated on $B220^+$ cells and Folli B on $B220^+IgM^{low}$ cells, followed by analysis. Apoptotic B cells in the spleen were detected with the B220 and Annexin V–FITC double-staining kit (BD). For analysis of the apoptotic populations of MCF-7, MDA-MB-231, and primary B cells, both early and late apoptotic cells were scored.

### FACS analysis

MCF-7 cells were cotransfected with pEGFP-N1 and AKT-CA at a mass ratio of 2:3 in a 6-cm dish. 12 h after transfection, cells were treated with PP242 (400 nM) or left untreated for an additional 24 h. Subsequently, cells were detached via trypsin treatment, pooled with the floating cell population (often at the late apoptotic stage), and resuspended in phenol-free DMEM as the base medium. The green fluorescent cell population of interest was gated based on light scatter and fluorescence on a FACSAria (BD).

### TUNEL staining

Tumor tissues were formalin fixed and paraffin embedded followed by TUNEL staining with the In Situ Cell Death Detection kit (Roche) according to the manufacturer's instructions. The percentage of apoptotic cells was estimated under a microscope.

### Statistical analysis

All statistical analyses were conducted using SPSS 13.0 software. Data are presented as mean values ± SEM of at least three independent experiments and analyzed using a two-tailed *t* test or one-way analysis of variance with multiple comparisons followed by Bonferroni post-hoc test for significance. A p-value $<0.05$ was considered statistically significant. Microscopic and Western blot images are representative of at least three independent experiments.

### Online supplemental material

Table S1 lists miRNAs that are differentially regulated by pp242 and rapamycin. Table S2 lists the sequences of ChIP RT-qPCR primers used in this study. Table S3 lists the sequences of the siRNAs and miRNAs used in this study. Table S4 lists the sequences of B cell KO mouse genotype primers used in this study. Table S5 lists the sequences of pMIR-reporters used in this study. Fig. S1 provides flow cytometry data to confirm the proapoptotic role of *miR-9-3p* and validates this role of *miR-9-3p* in other cell lines. Fig. S2 demonstrates that in contrast to *miR-9-3p*, *miR-9-5p* is a prosurvival miRNA. Fig. S3 provides additional data to confirm *miR-9-3p* acts downstream of mTORC2 and potentiates apoptosis by targeting E2F1. Fig. S4 shows that mTORC2

suppresses CIP2A expression and c-Myc phosphorylation at S62 in other cell lines. Fig. S5 shows that B cell–specific *Rictor* deletion mice grow normally but have a reduced splenic B cell number. Online supplemental material is available at http://www.jcb.org/cgi/content/full/jcb.201411128/DC1. Additional data are available in the JCB DataViewer at http://dx.doi.org/10.1083/jcb.201411128.dv.


### Acknowledgments

The authors appreciate the help of Dr. Rosalie Sears for providing us with the plasmids pD40-His-c-Myc, pD40-His-c-Myc$^{T58A}$, and pD40-His-c-Myc$^{S62A}$ and Mark A. Magnuson for providing *Rictor*$^{loxP/loxP}$ mice.

This study was supported by the National Natural Sciences Foundation of China (grants 81270088, 81301848, U1301222, and 31271271) and the Program for Changjiang Scholars and Innovative Research Team in University (grant IRT1142).

The authors declare no competing financial interests.

Submitted: 28 November 2014
Accepted: 27 August 2015


## References


AlQurashi, N., S.M. Hashimi, and M.Q. Wei. 2013. Chemical inhibitors and microRNAs (miRNA) targeting the mammalian target of rapamycin (mTOR) pathway: Potential for novel anticancer therapeutics. *Int. J. Mol. Sci.* 14:3874–3900. http://dx.doi.org/10.3390/ijms14023874

Askew, D.S., R.A. Ashmun, B.C. Simmons, and J.L. Cleveland. 1991. Constitutive c-myc expression in an IL-3-dependent myeloid cell line suppresses cell cycle arrest and accelerates apoptosis. *Oncogene.* 6:1915–1922.

Bai, X., and Y. Jiang. 2010. Key factors in mTOR regulation. *Cell. Mol. Life Sci.* 67:239–253. http://dx.doi.org/10.1007/s00018-009-0163-7

Benjamin, D., M. Colombi, C. Moroni, and M.N. Hall. 2011. Rapamycin passes the torch: A new generation of mTOR inhibitors. *Nat. Rev. Drug Discov.* 10:868–880. http://dx.doi.org/10.1038/nrd3531

Biswas, A.K., and D.G. Johnson. 2012. Transcriptional and nontranscriptional functions of E2F1 in response to DNA damage. *Cancer Res.* 72:13–17. http://dx.doi.org/10.1158/0008-5472.CAN-11-2196

Bronevetsky, Y., A.V. Villarino, C.J. Eisley, R. Barbeau, A.J. Barczak, G.A. Heinz, E. Kremmer, V. Heissmeyer, M.T. McManus, D.J. Erle, et al. 2013. T cell activation induces proteasomal degradation of Argonaute and rapid remodeling of the microRNA repertoire. *J. Exp. Med.* 210:417–432. http://dx.doi.org/10.1084/jem.20111717

Carew, J.S., K.R. Kelly, and S.T. Nawrocki. 2011. Mechanisms of mTOR inhibitor resistance in cancer therapy. *Target Oncol.* 6:17–27. http://dx.doi.org/10.1007/s11523-011-0167-8

Chen, P., C. Price, Z. Li, Y. Li, D. Cao, A. Wiley, C. He, S. Gurbuxani, R.B. Kunjamma, H. Huang, et al. 2013. miR-9 is an essential oncogenic microRNA specifically overexpressed in mixed lineage leukemia-rearranged leukemia. *Proc. Natl. Acad. Sci. USA.* 110:11511–11516. http://dx.doi.org/10.1073/pnas.1310144110

Clark, A.S., K. West, S. Streicher, and P.A. Dennis. 2002. Constitutive and inducible Akt activity promotes resistance to chemotherapy, trastuzumab, or tamoxifen in breast cancer cells. *Mol. Cancer Ther.* 1:707–717.

Dancey, J. 2010. mTOR signaling and drug development in cancer. *Nat Rev Clin Oncol.* 7:209–219. http://dx.doi.org/10.1038/nrclinonc.2010.21

Engelmann, D., and B.M. Pützer. 2012. The dark side of E2F1: In transit beyond apoptosis. *Cancer Res.* 72:571–575. http://dx.doi.org/10.1158/0008-5472.CAN-11-2575

Feldman, M.E., B. Apsel, A. Uotila, R. Loewith, Z.A. Knight, D. Ruggero, and K.M. Shokat. 2009. Active-site inhibitors of mTOR target rapamycin-resistant outputs of mTORC1 and mTORC2. *PLoS Biol.* 7:e38.

Gill, R.M., T.V. Gabor, A.L. Couzens, and M.P. Scheid. 2013. The MYC-associated protein CDCA7 is phosphorylated by AKT to regulate MYC-dependent apoptosis and transformation. *Mol. Cell. Biol.* 33:498–513. http://dx.doi.org/10.1128/MCB.00276-12

Heller, G., M. Weinzierl, C. Noll, V. Babinsky, B. Ziegler, C. Altenberger, C. Minichsdorfer, G. Lang, B. Döme, A. End-Pfützenreuter, et al. 2012. Genome-wide miRNA expression profiling identifies *miR-9-3* and *miR-193a* as targets for DNA methylation in non–small cell lung cancers. *Clin. Cancer Res.* 18:1619–1629. http://dx.doi.org/10.1158/1078-0432.CCR-11-2450

Huang, W.C., and M.C. Hung. 2009. Induction of Akt activity by chemotherapy confers acquired resistance. *J. Formos. Med. Assoc.* 108:180–194. http://dx.doi.org/10.1016/S0929-6646(09)60051-6

Hung, C.M., L. Garcia-Haro, C.A. Sparks, and D.A. Guertin. 2012. mTOR-dependent cell survival mechanisms. *Cold Spring Harb. Perspect. Biol.* 4:a008771. http://dx.doi.org/10.1101/cshperspect.a008771

Jacobsen, K.A., V.S. Prasad, C.L. Sidman, and D.G. Osmond. 1994. Apoptosis and macrophage-mediated deletion of precursor B cells in the bone marrow of E mu-myc transgenic mice. *Blood.* 84:2784–2794.

Jeon, H.M., Y.W. Sohn, S.Y. Oh, S.H. Kim, S. Beck, S. Kim, and H. Kim. 2011. ID4 imparts chemoresistance and cancer stemness to glioma cells by derepressing miR-9*–mediated suppression of SOX2. *Cancer Res.* 71:3410–3421. http://dx.doi.org/10.1158/0008-5472.CAN-10-3340

Jewell, J.L., R.C. Russell, and K.L. Guan. 2013. Amino acid signalling upstream of mTOR. *Nat. Rev. Mol. Cell Biol.* 14:133–139. http://dx.doi.org/10.1038/nrm3522

Jin, Y., S.D. Tymen, D. Chen, Z.J. Fang, Y. Zhao, D. Dragas, Y. Dai, P.T. Marucha, and X. Zhou. 2013. MicroRNA-99 family targets AKT/mTOR signaling pathway in dermal wound healing. *PLoS One.* 8:e64434. http://dx.doi.org/10.1371/journal.pone.0064434

Johnson, S.C., P.S. Rabinovitch, and M. Kaeberlein. 2013. mTOR is a key modulator of ageing and age-related disease. *Nature.* 493:338–345. http://dx.doi.org/10.1038/nature11861

Junttila, M.R., P. Puustinen, M. Niemelä, R. Ahola, H. Arnold, T. Böttzauw, R. Ala-aho, C. Nielsen, J. Ivaska, Y. Taya, et al. 2007. CIP2A inhibits PP2A in human malignancies. *Cell.* 130:51–62. http://dx.doi.org/10.1016/j.cell.2007.04.044

Knuefermann, C., Y. Lu, B. Liu, W. Jin, K. Liang, L. Wu, M. Schmidt, G.B. Mills, J. Mendelsohn, and Z. Fan. 2003. HER2/PI-3K/Akt activation leads to a multidrug resistance in human breast adenocarcinoma cells. *Oncogene.* 22:3205–3212. http://dx.doi.org/10.1038/sj.onc.1206394

Kovala, A.T., K.A. Harvey, P. McGlynn, G. Boguslawski, J.G. Garcia, and D. English. 2000. High-efficiency transient transfection of endothelial cells for functional analysis. *FASEB J.* 14:2486–2494. http://dx.doi.org/10.1096/fj.00-0147com

Krek, A., D. Grün, M.N. Poy, R. Wolf, L. Rosenberg, E.J. Epstein, P. MacMenamin, I. da Piedade, K.C. Gunsalus, M. Stoffel, and N. Rajewsky. 2005. Combinatorial microRNA target predictions. *Nat. Genet.* 37:495–500. http://dx.doi.org/10.1038/ng1536

Kurokawa, M., J. Kim, J. Geradts, K. Matsuura, L. Liu, X. Ran, W. Xia, T.J. Ribar, R. Henao, M.W. Dewhirst, et al. 2013. A network of substrates of the E3 ubiquitin ligases MDM2 and HUWE1 control apoptosis independently of p53. *Sci. Signal.* 6:ra32. http://dx.doi.org/10.1126/scisignal.2003741

Ladu, S., D.F. Calvisi, E.A. Conner, M. Farina, V.M. Factor, and S.S. Thorgeirsson. 2008. E2F1 inhibits c-Myc-driven apoptosis via PIK3CA/Akt/mTOR and COX-2 in a mouse model of human liver cancer. *Gastroenterology.* 135:1322–1332. http://dx.doi.org/10.1053/j.gastro.2008.07.012

Laplante, M., and D.M. Sabatini. 2012. mTOR signaling in growth control and disease. *Cell.* 149:274–293. http://dx.doi.org/10.1016/j.cell.2012.03.017

Lee, K., L. Heffington, J. Jellusova, K.T. Nam, A. Raybuck, S.H. Cho, J.W. Thomas, R.C. Rickert, and M. Boothby. 2013. Requirement for Rictor in homeostasis and function of mature B lymphoid cells. *Blood.* 122:2369–2379. http://dx.doi.org/10.1182/blood-2013-01-477505

Letai, A., M.D. Sorcinelli, C. Beard, and S.J. Korsmeyer. 2004. Antiapoptotic BCL-2 is required for maintenance of a model leukemia. *Cancer Cell.* 6:241–249. http://dx.doi.org/10.1016/j.ccr.2004.07.011

Ma, X.M., and J. Blenis. 2009. Molecular mechanisms of mTOR-mediated translational control. *Nat. Rev. Mol. Cell Biol.* 10:307–318. http://dx.doi.org/10.1038/nrm2672

Ma, L., J. Young, H. Prabhala, E. Pan, P. Mestdagh, D. Muth, J. Teruya-Feldstein, F. Reinhardt, T.T. Onder, S. Valastyan, et al. 2010. miR-9, a MYC/MYCN-activated microRNA, regulates E-cadherin and cancer metastasis. *Nat. Cell Biol.* 12:247–256.

Martinez, L.A., E. Goluszko, H.Z. Chen, G. Leone, S. Post, G. Lozano, Z. Chen, and A. Chauchereau. 2010. E2F3 is a mediator of DNA damage-induced apoptosis. *Mol. Cell. Biol.* 30:524–536. http://dx.doi.org/10.1128/MCB.00938-09

McMahon, S.B. 2014. MYC and the control of apoptosis. *Cold Spring Harb Perspect Med.* 4:a014407. http://dx.doi.org/10.1101/cshperspect.a014407

Muller, P.A., and K.H. Vousden. 2014. Mutant p53 in cancer: New functions and therapeutic opportunities. *Cancer Cell.* 25:304–317. http://dx.doi.org/10.1016/j.ccr.2014.01.021

Neiman, P.E., S.J. Thomas, and G. Loring. 1991. Induction of apoptosis during normal and neoplastic B-cell development in the bursa of Fabricius. *Proc. Natl. Acad. Sci. USA.* 88:5857–5861. http://dx.doi.org/10.1073/pnas.88.13.5857

Oh, W.J., and E. Jacinto. 2011. mTOR complex 2 signaling and functions. *Cell Cycle.* 10:2305–2316. http://dx.doi.org/10.4161/cc.10.14.16586

Okamura, K., N. Liu, and E.C. Lai. 2009. Distinct mechanisms for microRNA strand selection by *Drosophila* Argonautes. *Mol. Cell.* 36:431–444. http://dx.doi.org/10.1016/j.molcel.2009.09.027

Ozdek, A., S. Sarac, M.U. Akyol, A. Sungur, and T. Yilmaz. 2004. c-myc and bcl-2 expression in supraglottic squamous cell carcinoma of the larynx. *Otolaryngol. Head Neck Surg.* 131:77–83. http://dx.doi.org/10.1016/j.otohns.2004.02.015

Pei, H., L. Li, B.L. Fridley, G.D. Jenkins, K.R. Kalari, W. Lingle, G. Petersen, Z. Lou, and L. Wang. 2009. FKBP51 affects cancer cell response to chemotherapy by negatively regulating Akt. *Cancer Cell.* 16:259–266. http://dx.doi.org/10.1016/j.ccr.2009.07.016

Pencheva, N., and S.F. Tavazoie. 2013. Control of metastatic progression by microRNA regulatory networks. *Nat. Cell Biol.* 15:546–554. http://dx.doi.org/10.1038/ncb2769

Pützer, B.M., and D. Engelmann. 2013. E2F1 apoptosis counterattacked: Evil strikes back. *Trends Mol. Med.* 19:89–98. http://dx.doi.org/10.1016/j.molmed.2012.10.009

Rohn, J.L., A.O. Hueber, N.J. McCarthy, D. Lyon, P. Navarro, B.M. Burgering, and G.I. Evan. 1998. The opposing roles of the Akt and c-Myc signalling pathways in survival from CD95-mediated apoptosis. *Oncogene.* 17:2811–2818. http://dx.doi.org/10.1038/sj.onc.1202393

Sarbassov, D.D., S.M. Ali, D.H. Kim, D.A. Guertin, R.R. Latek, H. Erdjument-Bromage, P. Tempst, and D.M. Sabatini. 2004. Rictor, a novel binding partner of mTOR, defines a rapamycin-insensitive and raptor-independent pathway that regulates the cytoskeleton. *Curr. Biol.* 14:1296–1302. http://dx.doi.org/10.1016/j.cub.2004.06.054

Sarbassov, D.D., D.A. Guertin, S.M. Ali, and D.M. Sabatini. 2005. Phosphorylation and regulation of Akt/PKB by the rictor-mTOR complex. *Science.* 307:1098–1101. http://dx.doi.org/10.1126/science.1106148

Sellers, W.R., B.G. Novitch, S. Miyake, A. Heith, G.A. Otterson, F.J. Kaye, A.B. Lassar, and W.G. Kaelin Jr. 1998. Stable binding to E2F is not required for the retinoblastoma protein to activate transcription, promote differentiation, and suppress tumor cell growth. *Genes Dev.* 12:95–106. http://dx.doi.org/10.1101/gad.12.1.95

Shi, Y., J.M. Glynn, L.J. Guilbert, T.G. Cotter, R.P. Bissonnette, and D.R. Green. 1992. Role for c-myc in activation-induced apoptotic cell death in T cell hybridomas. *Science.* 257:212–214. http://dx.doi.org/10.1126/science.1378649

Sparks, C.A., and D.A. Guertin. 2010. Targeting mTOR: Prospects for mTOR complex 2 inhibitors in cancer therapy. *Oncogene.* 29:3733–3744. http://dx.doi.org/10.1038/onc.2010.139

Stanelle, J., and B.M. Pützer. 2006. E2F1-induced apoptosis: Turning killers into therapeutics. *Trends Mol. Med.* 12:177–185. http://dx.doi.org/10.1016/j.molmed.2006.02.002

Sun, Y., Y. Ge, J. Drnevich, Y. Zhao, M. Band, and J. Chen. 2010. Mammalian target of rapamycin regulates miRNA-1 and follistatin in skeletal myogenesis. *J. Cell Biol.* 189:1157–1169. http://dx.doi.org/10.1083/jcb.200912093

Thum, T., C. Gross, J. Fiedler, T. Fischer, S. Kissler, M. Bussen, P. Galuppo, S. Just, W. Rottbauer, S. Frantz, et al. 2008. MicroRNA-21 contributes to myocardial disease by stimulating MAP kinase signalling in fibroblasts. *Nature.* 456:980–984. http://dx.doi.org/10.1038/nature07511

Totary-Jain, H., and A.R. Marks. 2013. MicroRNAs and the cellular response to rapamycin: Potential role in diagnosis and therapy. *Cell Cycle.* 12:861–862. http://dx.doi.org/10.4161/cc.24100

Totary-Jain, H., D. Sanoudou, I.Z. Ben-Dov, C.N. Dautriche, P. Guarnieri, S.O. Marx, T. Tuschl, and A.R. Marks. 2013. Reprogramming of the microRNA transcriptome mediates resistance to rapamycin. *J. Biol. Chem.* 288:6034–6044. http://dx.doi.org/10.1074/jbc.M112.416446

Trindade, A.J., D.A. Medvetz, N.A. Neuman, F. Myachina, J. Yu, C. Priolo, and E.P. Henske. 2013. MicroRNA-21 is induced by rapamycin in a model of tuberous sclerosis (TSC) and lymphangioleiomyomatosis (LAM). *PLoS One.* 8:e60014. http://dx.doi.org/10.1371/journal.pone.0060014

Uesugi, A., K. Kozaki, T. Tsuruta, M. Furuta, K. Morita, I. Imoto, K. Omura, and J. Inazawa. 2011. The tumor suppressive microRNA miR-218 targets the mTOR component Rictor and inhibits AKT phosphorylation in oral cancer. *Cancer Res.* 71:5765–5778. http://dx.doi.org/10.1158/0008-5472.CAN-11-0368

Wahlquist, C., D. Jeong, A. Rojas-Muñoz, C. Kho, A. Lee, S. Mitsuyama, A. van Mil, W.J. Park, J.P. Sluijter, P.A. Doevendans, et al. 2014. Inhibition of *miR-25* improves cardiac contractility in the failing heart. *Nature.* 508:531–535. http://dx.doi.org/10.1038/nature13073

Walker, S.M., G.C. Meinke, and W.O. Weigle. 1979. Separation of various B-cell subpopulations from mouse spleen. I. Depletion of B cells by rosetting with glutaraldehyde-fixed, anti-immunoglobulin-coupled red blood cells. *Cell. Immunol.* 46:158–169. http://dx.doi.org/10.1016/0008-8749(79)90253-3

Wander, S.A., B.T. Hennessy, and J.M. Slingerland. 2011. Next-generation mTOR inhibitors in clinical oncology: How pathway complexity informs therapeutic strategy. *J. Clin. Invest.* 121:1231–1241. http://dx.doi.org/10.1172/JCI44145

Westmoreland, J.J., Q. Wang, M. Bouzaffour, S.J. Baker, and B. Sosa-Pineda. 2009. Pdk1 activity controls proliferation, survival, and growth of developing pancreatic cells. *Dev. Biol.* 334:285–298. http://dx.doi.org/10.1016/j.ydbio.2009.07.030

Wyllie, A.H., K.A. Rose, R.G. Morris, C.M. Steel, E. Foster, and D.A. Spandidos. 1987. Rodent fibroblast tumours expressing human myc and ras genes: Growth, metastasis and endogenous oncogene expression. *Br. J. Cancer.* 56:251–259. http://dx.doi.org/10.1038/bjc.1987.186

Yeh, E., M. Cunningham, H. Arnold, D. Chasse, T. Monteith, G. Ivaldi, W.C. Hahn, P.T. Stukenberg, S. Shenolikar, T. Uchida, et al. 2004. A signalling pathway controlling c-Myc degradation that impacts oncogenic transformation of human cells. *Nat. Cell Biol.* 6:308–318. http://dx.doi.org/10.1038/ncb1110

Yeh, E.S., G.K. Belka, A.E. Vernon, C.C. Chen, J.J. Jung, and L.A. Chodosh. 2013. Hunk negatively regulates c-myc to promote Akt-mediated cell survival and mammary tumorigenesis induced by loss of *Pten*. *Proc. Natl. Acad. Sci. USA.* 110:6103–6108. http://dx.doi.org/10.1073/pnas.1217415110

Yuva-Aydemir, Y., A. Simkin, E. Gascon, and F.B. Gao. 2011. MicroRNA-9: Functional evolution of a conserved small regulatory RNA. *RNA Biol.* 8:557–564. http://dx.doi.org/10.4161/rna.8.4.16019

Zawistowski, J.S., K. Nakamura, J.S. Parker, D.A. Granger, B.T. Golitz, and G.L. Johnson. 2013. MicroRNA 9-3p targets $\beta_1$ integrin to sensitize claudin-low breast cancer cells to MEK inhibition. *Mol. Cell. Biol.* 33:2260–2274. http://dx.doi.org/10.1128/MCB.00269-13

Zheng, C., Z. Ren, H. Wang, W. Zhang, D.V. Kalvakolanu, Z. Tian, and W. Xiao. 2009. E2F1 Induces tumor cell survival via nuclear factor-κB–dependent induction of EGR1 transcription in prostate cancer cells. *Cancer Res.* 69:2324–2331. http://dx.doi.org/10.1158/0008-5472.CAN-08-4113

Zindy, F., C.M. Eischen, D.H. Randle, T. Kamijo, J.L. Cleveland, C.J. Sherr, and M.F. Roussel. 1998. Myc signaling via the ARF tumor suppressor regulates p53-dependent apoptosis and immortalization. *Genes Dev.* 12:2424–2433. http://dx.doi.org/10.1101/gad.12.15.2424